



Practical insights on standardised models for estimation of crack width due to imposed strains in edge-restrained reinforced concrete elements

Agnieszka Jędrzejewska, Mariusz Zych, Jean Michel Torrenti, Fragkoulis Kanavaris, Miguel Azenha, Fangjie Chen, Shintaro Ito

► To cite this version:

Agnieszka Jędrzejewska, Mariusz Zych, Jean Michel Torrenti, Fragkoulis Kanavaris, Miguel Azenha, et al.. Practical insights on standardised models for estimation of crack width due to imposed strains in edge-restrained reinforced concrete elements. Engineering Structures, 2024, 305, pp.117757. 10.1016/j.engstruct.2024.117757 . hal-04493430

HAL Id: hal-04493430

<https://hal.science/hal-04493430>

Submitted on 13 Mar 2024

HAL is a multi-disciplinary open access archive for the deposit and dissemination of scientific research documents, whether they are published or not. The documents may come from teaching and research institutions in France or abroad, or from public or private research centers.

L'archive ouverte pluridisciplinaire **HAL**, est destinée au dépôt et à la diffusion de documents scientifiques de niveau recherche, publiés ou non, émanant des établissements d'enseignement et de recherche français ou étrangers, des laboratoires publics ou privés.

Practical insights on standardised models for estimation of crack width due to imposed strains in edge-restrained reinforced concrete elements

Agnieszka Jędrzejewska^{a,*}, Mariusz Zych^b, Jean Michel Torrenti^c, Fragkoulis Kanavaris^d, Miguel Azenha^e, Fangjie Chen^f, Shintaro Ito^g

^a Silesian University of Technology, Department of Structural Engineering, Akademicka 5, 44-100 Gliwice, Poland

agnieszka.jedrzejewska@polsl.pl

^b Cracow University of Technology, Reinforced Concrete Structures Division, Warszawska 24, 31-155 Kraków, Poland

mzych@pk.edu.pl

^c Université Gustave Eiffel, Department of Materials and Structures, 16 Bd Newton, 77420 Champs-sur-Marne, France

jean-michel.torrenti@univ-eiffel.fr

^d ARUP, 8-13 Fitzroy St, London W1T 4BQ, UK

frag.kanavaris@arup.com

^e University of Minho, ISISE, ARISE, Department of Civil Engineering, 4800-058 Guimarães, Portugal

miguel.azenha@civil.uminho.pt

^f ARUP, Sky Park, 1 Melbourne Quarter, 699 Collins St, Docklands VIC 3008, Australia

sam.chen@arup.com

^g ARUP, 8F Iidabashi Grand Bloom, 2-10-2 Fujimi Chiyoda-ku, Tokyo 102-0071, Japan

shintaro.ito@arup.com

* corresponding author; contact address: Agnieszka.Jedrzejewska@polsl.pl

Abstract. The paper presents a critical study on the predictive capacity of standardised methods for crack width calculations in edge-restrained reinforced concrete elements subjected to imposed strains. The aim of the presented integrative analysis was to reach global understanding of the issue of restraint-induced cracking from the point of view of SLS design and to build a sound basis for future developments of new models. The study covered relevant methods from Europe, Australia, Japan and the USA. The study was performed on three distinct case studies: (i) a demonstration example; (ii) a massive containment wall; and (iii) a heavily-reinforced tank wall segment. It was concluded that a model for crack width control in edge-restrained elements should consider the stage of cracking and be generalised for possible geometries and reinforcement. Agreement must be made on the properties of concrete applied in the design, including effective tensile strength, effective modulus of elasticity (to account for creep) and the level of strain relieve after crack formation with its effect on the crack width.

Keywords: crack control; standards; imposed strains; crack width; wall-on-slab; restraint.

1 Introduction

The aim of the serviceability limit state (SLS) design of cracking of reinforced concrete structures is predominately to ensure durability of the structure but also to ensure its functionality. Crack width control is especially important in structures with increased tightness requirements: water tightness or restricted permeability [1]. These include structures in direct contact with ground water, such as retaining walls, tunnels and bridge abutments, as well as tanks and various types of nuclear containments. In addition to external mechanical loading acting during operation, these structures are also subjected to the action of imposed strains. These imposed strains result from the effect of temperature changes, shrinkage and creep, and may occur over the whole life of the structure, both at the construction stage (autogenous shrinkage and temperature variation resulting from cement hydration during hardening of concrete) and during operation (drying shrinkage and temperature variations resulting from ambient temperature or service conditions) [2].

The design for restraint-induced cracking in reinforced concrete structures is a challenging endeavour. It consists in general of three tasks: (i) quantification of imposed strains, (ii) assessment of the restraining conditions, and (iii) determination of the required reinforcement for crack width control. In design guidelines, the restraint is usually differentiated into **internal** and **external** restraint. In case of the latter, a distinction should be made into (i) **end restraint**, where an element is externally restrained at its extremities, (ii) **edge restraint**, where an element is externally restrained along its edge, usually the base, and (iii) **combined restraint** where an element is restrained along multiple edges. This paper focuses on the SLS design of the edge-restrained elements which represent a range of the wall structures, majority of which are the structures with the increased tightness requirements.

Even though there exist design methods throughout the engineering community (some of which have been implemented into design guidelines and standards), there is no agreement on the formulation for the crack width calculation in reinforced concrete elements subjected to the restraint-induced cracking.

A systematic overview was needed of the available methods. So far, such state-of-the-art studies have been done for crack width estimation methods in flexural elements, see e.g. the works of *Borosnyói and Balazs* [3] or more recent work of *Lapi et al.* [4]. Chosen standardised methods for crack width

calculations in wall structures (EN 1992-1-1:2004 [5] & EN 1992-3:2006 [6], CIRIA C660 [7], ACI 207.2 [8] and JCI Guideline [9]) have been comparatively studied by *Klemczak and Žmij* [10]. A review on the crack width estimations in edge-restrained elements according to these guidelines has been also done by *Zych* [11] in addition to the analysis of various non-standardised analytical models. Finally, an extensive review of the standardised methods for the restraint-induced cracking of reinforced concrete structures has been presented by the authors in [12]. The comparative study covered all relevant design methods implemented in the guidelines worldwide, and included European standards: EN 1992-1-1:2004 [5], EN 1992-3:2006 [6] and the latest available at the time version of the final draft FprEN 1992-1-1 [13] (now issued with minor changes as an official version EN 1992-1-1:2023 [14]), as well as British guideline CIRIA C766 [15]; Australian recommendations CIA Z7/06 [16]; Japanese recommendations AIJ-SRC **Erreur ! Source du renvoi introuvable.**, and American ACI reports 207.2R-07 [8] and 224R-01 [18], and covered both end-restrained and edge-restrained elements.

The overview of the design methods showed that the main difference between the methods lays in the assumptions of the model. There exist proposals based purely on the empirical or experimental bases, and these have not been implemented for design [11]. The current version of the JCI Guideline is, in turn, fully based on the extensive FEM-based calculations and thus has no direct physical meaning, as explained by the authors in [12]. Regarding the standardised methods, majority of the currently used guidelines, namely those following the philosophy of EN 1992-1-1:2004 [5], assume the same bond strength for the crack formation stage and stabilised cracking stage, which results in the same value of the transfer length in both cracking stages, although for the crack formation stage the calculated $s_{r,max}$ should be interpreted as twice the transfer length ($s_{r,max} = 2l_{e,max}$) while for the stabilised cracking as the crack spacing. The same models for crack spacing as for the elements in direct tension are recommended for the design of the elements subjected to the restraint of imposed strains. Only some of the design guidelines explicitly acknowledge the fact that the cracking caused by the restraint of imposed strains is governed by the single-crack condition (crack formation phase). These include AIJ-SRC [17] and the design method implemented in the ACI 207.2-95 [19], which is no longer a valid standard. The differences in the methods result also from the way in which the values of relevant input

parameters are determined in the method. This relates to the magnitude of the imposed strains, effective tensile strength, reinforcement ratio, effect of creep and degree of restraint.

Consequently, experience of the authors has shown that crack width estimates may vary significantly depending on which model is used, however, no systematic studies comparing the predictive capacities of the methods have been identified in the literature. In general, the comparative studies are usually limited to a given group of models based on the same philosophy where calibrations are proposed to modify the models to obtain better compliance between the experimental measurements and calculation results. Among numerous studies, one can mention the works comparing the past version of EN 1992-3:2006 and CIRIA C766 in their predictive capacity to evaluate the expected crack widths in edge-restrained walls, such as the study of *El Khoury et al.* [20] on laboratory tests of mock-up walls or the study of *Jędrzejewska et al.* [1] on the experiences from in-situ cracking of wall-on-slab structures. Both works indicated significant discrepancies of both approaches regarding the compliance of the measurements and calculations. Analogous comparisons have been made between the previous and new version of EN 1992 as well as between FprEN 1992-1-1 and CIRIA C766 by e.g. *Klausen* [21], as the main aim of the new guidelines of Eurocode 2 has been to improve the predictive capacity of the model initially proposed in EN 1992-1-1:2004 & EN 1992-3:2006. Nevertheless, the performance of the EN 1992-1-1:2023 [14] model on real-scale wall-type structures has not yet been investigated. Here, one should also mention the extensive study performed by CROW-CUR in the Netherlands where a modification to the EN 1992-1-1:2004 [5] formula for crack spacing has been proposed based on the analysis of cracking observed in-situ on a large set of real-life structures. In the approach proposed in the CROW-CUR report [22] the component related to the concrete cover was removed following the philosophy of the German National Annex to EN 1992-1-1 [23].

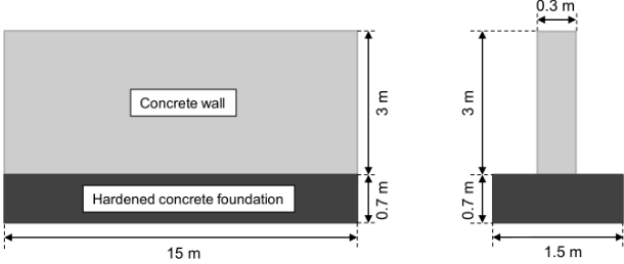
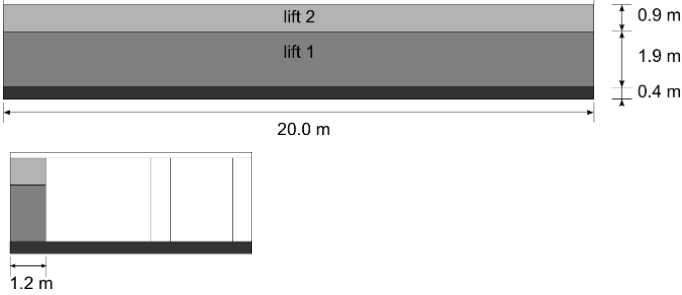
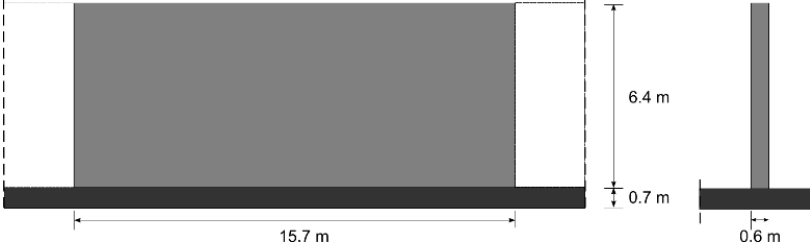
As mentioned earlier, a broader study based on in-situ measurements of the walls has been performed by *Klemczak and Żmij* [10]. Nevertheless, new versions of the guidelines analysed in this study have been issued which include significant modifications and thus deserve re-addressing. Most importantly, however, the focus of this comparative study was rather on the easiness of use, not the physical background of the model assumptions. Regarding the methods which are derived from the assumption of crack-formation stage, comparative studies were performed by *Carino and Clifton* [24] for the

methods of *Gilbert* [25] (implemented in CIA Z7/06 [16]) and *Base and Murray* [26] (whose modified version is implemented in AIJ-SRC recommendations [16]) but only for the end-restrained elements. The modified Base–Murray method implemented in AIJ-SRC guideline, which is the only example of the method developed originally for the elements under imposed strains accounting for the stage of cracking, has never been compared with the modified methods originating from the models for the elements under direct tension (Eurocode 2 and ACI 207/224). This leaves an open question whether its mechanically sound philosophy makes this approach superior to the other methods regarding its performance in crack width estimation.

Therefore, in this paper a *benchmark* type of investigation has been performed with the aim to evaluate the discrepancies in the restraint-induced crack width calculated from different codified models around the world. First, estimates of the crack width for given reinforcement as well as the required reinforcement to limit the crack width were made on a theoretical example of a wall-on-slab structure; this also allowed to perform a sensitivity analysis of the methods. Second, the methods were validated against two real-life case studies, which were comprehensively monitored for temperature, strains and crack characteristics: a nuclear containment wall and a tank wall segment. Table 1 summarises the analysed benchmark case studies – their nature and key takeaway conclusions.

The aim of this research was therefore to perform an integrative analysis of several approaches which are intended to be inherently wide yet relatively simple to use for design purposes, and consequently to reach global understanding of the phenomenon of restraint-induced cracking. As an effect, the authors define the ranges of applicability of the currently used models and their limitations, providing useful guidelines for the design with the use of these models, given the particularities of the design of the structures subjected to the restraint of imposed strains. Moreover, a sound and solid basis is built for conceptualisation of new models, whose development is needed to overcome the deficiencies of the current solutions, such as the proposals of *Schlicke et al.* [27], *Tan et al.* [28] or *Somma et al.* [29].

Table 1. Summary of the analysed case studies.

CASE STUDY	Nature of the example and level of information available	Purpose of the study
<p>Wall-on-slab structure (Section 3)</p> 	<p>Theoretical example representing a typical semi-massive base-restrained wall on foundation. All the input data are assumed as realistic probable values. This example is used for comparative study and sensitivity analysis of the analysis methods.</p>	<p>Basic understanding of differences of in the analysed models.</p>
<p>Massive wall of Civaux NPP mock-up (Section 4)</p> 	<p>Real-life case study. Only early-age cracking (due to hydration and early shrinkage). Input data: geometry, materials, reinforcement, measurements of temperature (in-situ) and shrinkage (laboratory), measurements of crack spacing and crack width after 5 days.</p>	<p>Predictive capacity of the models in estimation of the magnitude of early-age imposed strains, crack spacing and crack width in crack-formation stage. Study on the influence of massivity/cross-sectional dimensions.</p>
<p>Heavily reinforced tank wall segment (Section 5)</p> 	<p>Real-life case study. Cracking due to both early-age and long-term imposed strains. Input data: geometry, materials, reinforcement, measurements of total strains (in-situ), temperature (in-situ), shrinkage (laboratory), crack spacing and crack width after 16 days, 90 days and 9 months.</p>	<p>Predictive capacity of the models in estimation of the crack spacing and crack width change in time (from early-age to long-term) with changing imposed strains.</p>

2 Restraint-induced cracking in edge-restrained elements

2.1 Characterisation of cracking in walls

Cracking behaviour of edge-restrained structures, such as walls on slabs, have been characterised by the authors based on a study of a collection of real-life examples of cracked wall-on-slab structures [1]. The stresses in these structural elements are generated due to eccentric restraint of potential elongation/shortening of the wall by the restraining element (foundation or other adjacent element, e.g., neighbouring segment or lift). The decisive stress distribution varies throughout the structure and depends on the magnitude of the imposed strains in the wall, stiffness ratios between the wall and restraining body as well as the length-to-height ratio of the wall, i.e., a ratio relevant to a potential cracking pattern. When the tensile capacity of concrete of the wall is reached, tensile stresses lead to formation of cracks. In the simplest case of a base-restrained element, the first crack appears theoretically at half length of the wall, near the joint with the underlying foundation, and develops toward the top edge of the wall. This crack can be followed by other cracks, which appear at a certain distance from one another and reach a certain height. The final cracking pattern depends on the number of factors including those described before, as well as on the support conditions (number of restrained edges). The following factors were identified to influence the cracking potential and cracking pattern in the edge-restrained elements subjected to imposed strains [1]:

1. **Massivity of the element** which is a measure of proneness of the structure to either thermal or shrinkage cracking as well as of the share of self-induced and restraint stresses in the crack risk assessment and cracking pattern characterisation.
2. **Mix composition** which in combination with the massivity of the element and curing conditions, influences the magnitude of the imposed strains at early age. Optimum mix design is of special importance in externally-restrained elements due to the inherent trade-off between decreasing the imposed strains – especially thermal strains – and maintaining relatively fast development of strength.

3. **Degree of external restraint** which determines the magnitude of stress-effective (restrained) part of imposed strain, expressed by means of the length-to-height ratio of the restrained element as well as its relative stiffness with respect to the restraining element.
4. **Support conditions** – the number of restrained edges – which determines the pattern of cracks: their location, range, spacing and shape. For the base-restrained elements, cracks are vertical and the highest along the centreline and decrease in height and slant towards free edges. The number of restrained edges (base only / base + 1 side / base + 2 sides) has no direct effect on the width of the cracks, only influences their amount and range.
5. **Reinforcement** – horizontal reinforcement is of interest for restraint-induced cracking in walls. Naturally, higher reinforcement ratio allows to limit the width of the cracks and their spacing, however, the efficiency of reinforcement in limiting the crack widths decreases with an increasing reinforcement ratio. Furthermore, for low reinforcement ratios ($< 0.7\%$), especially close to the minimum reinforcement, high variability and randomness of crack widths is observed, as the activated reinforcement in the vicinity of the crack may reach very high strains with significant deterioration of bond properties and there is no control of cracking.

2.2 Crack width estimation in design guidelines

The crack width in an edge-restrained element can basically be expressed by the product of the length in which concrete slips on the reinforcement at both sides of the crack ($2l_e$), and the difference of the mean strain between steel and concrete ($\varepsilon_{sm} - \varepsilon_{cm}$), which is referred to as the crack-inducing strain, ε_{cr} . The same bond strength is assumed regardless of the stage of cracking (crack formation stage or stabilised cracking stage) as well as that stabilised crack spacing is reached when $s_r = 2l_e$. That is why the component of twice the transfer length is often simplified by the crack spacing. In edge-restrained elements, cracking changes internal forces only locally and the strain difference depends on the restrained part of strain of the uncracked section. Consequently, the value of the crack-inducing strain is expressed the part of the restrained strain that is relieved by forming cracks and is equal to the restrained part of imposed strain $\varepsilon_{rest} = R \cdot \varepsilon_{imp}$ minus the average tensile strain in the concrete after cracking, which is related to the portion of its tensile capacity $k_t \cdot \varepsilon_{ctu}$:

$$w = s_r \cdot (\varepsilon_{sm} - \varepsilon_{cm}) = s_r \cdot \varepsilon_{cr} = s_r \cdot (\varepsilon_{rest} - k_t \cdot \varepsilon_{ctu}) \quad (1)$$

Table 2 summarises the formulas in the crack width calculations for edge-restrained elements with different standardised methods, discussed in [12]. In all cases crack spacing is derived from the model of a tie: the edge-restrained elements are represented as ties in which the fixation at the extremities is replaced with an actual degree of restraint described with the restraint factor. This is graphically explained in Fig. 1a. Majority of the methods treat the whole wall as a single tie and use the maximum value of the restraint factor at the height for the design. ACI 207.2 [8] acknowledges the fact that the degree of restraint in an edge-restrained element decreases towards the free edge and allows to differentiate the required reinforcement ratio at the height of the wall by dividing the wall into sub-ties (lifts) with decreasing value of the restraint factor.

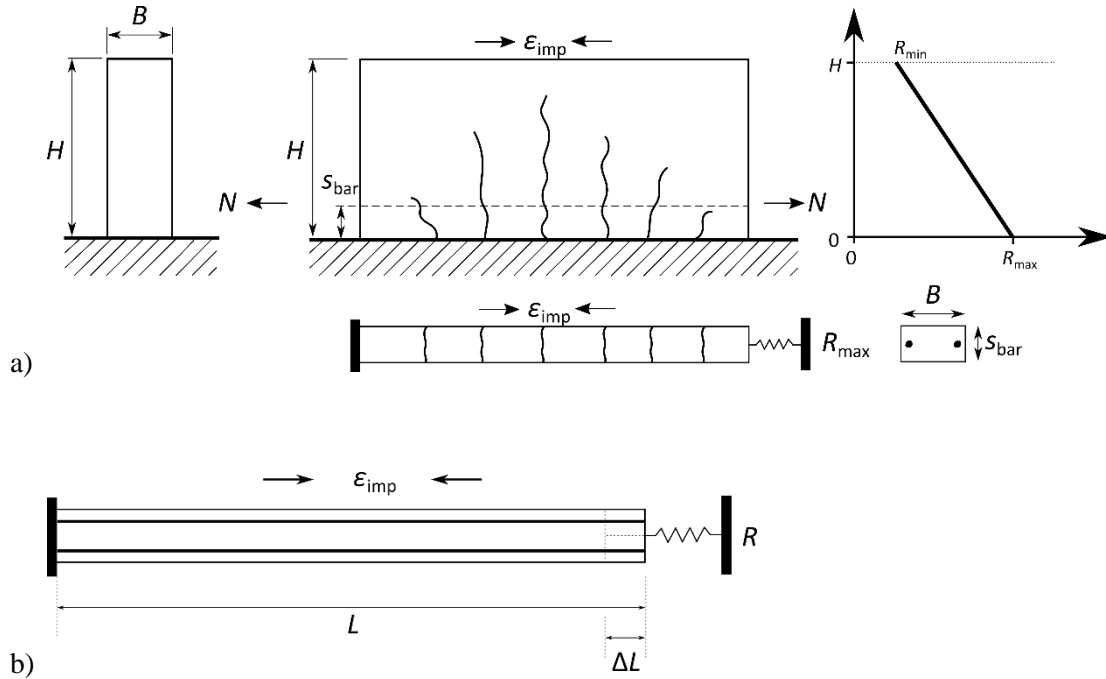


Figure 1. Graphical explanation of the method for SLS design of cracking of edge-restrained elements subjected to imposed deformations with the use of an equivalent tie model: (a) definition of the model; (b) compatibility of deformations.

2.3 Degree of restraint and restraint factor

One of the key parameters in crack width control of edge-restrained elements is the degree of restraint conventionally represented with a restraint factor, R . Discrepancies can be noted between the methods in the definition of the degree of restraint and restrained part of strain, especially in the meaning of ε_{imp}

and $\varepsilon_{\text{free}}$. Therefore, the authors found it crucial to unify the denotations throughout the methods in this paper to facilitate their use for the designer. These unified denotations have been introduced in Fig. 1b, and used in the presentation of the methods in Table 2 and throughout the paper.

Figure 1b illustrates the conditions of deformations compatibility in a partially-restrained tie which is subjected to imposed strain ε_{imp} . The source of this imposed strain might be temperature drop and/or shrinkage of concrete. Due to partial restraint of the element, a part of this strain will cause deformation of an element, and a strain related to this deformation is a free part of imposed strain, $\varepsilon_{\text{free}} = \Delta L/L$. The remaining part of the strain is, in turn, a restrained strain $\varepsilon_{\text{rest}}$, so $\varepsilon_{\text{imp}} = \varepsilon_{\text{free}} + \varepsilon_{\text{rest}}$. The magnitude of the restrained strain depends on the degree of restraint, R , which can thus be defined as:

$$R = \frac{\varepsilon_{\text{rest}}}{\varepsilon_{\text{imp}}} = \frac{\varepsilon_{\text{imp}} - \varepsilon_{\text{free}}}{\varepsilon_{\text{imp}}} = 1 - \frac{\varepsilon_{\text{free}}}{\varepsilon_{\text{imp}}} \quad (2)$$

Hence, with the use of the degree of restraint, the restrained part of imposed strain can be expressed as $\varepsilon_{\text{rest}} = R \cdot \varepsilon_{\text{imp}}$.

code	crack spacing s_r	crack-inducing strain $\varepsilon_{cr} = \varepsilon_{sm} - \varepsilon_{cm}$	crack width
EN 1992-1-1:2004 & EN 1992-3:2006	$s_{r,max} = 3.4 \cdot c + 0.425 \cdot k_1 \cdot k_2 \cdot \frac{\phi}{\rho_{eff}}$ $k_1 = 0.8$ for good bond	$\varepsilon_{cr} = \varepsilon_{rest} = R_{ax} \cdot \varepsilon_{imp}$	$w_{max} = s_{r,max} \cdot (\varepsilon_{sm} - \varepsilon_{cm})$
CIRIA C766	$s_{r,max} = 3.4 \cdot c + 0.425 \cdot k_1 \cdot k_2 \cdot \frac{\phi}{\rho_{eff}}$ $k_1 = 1.14$ for poor bond (at early age)	$\varepsilon_{cr} = \varepsilon_{rest} - 0.5\varepsilon_{ctu} = R \cdot \varepsilon_{imp} - 0.5\varepsilon_{ctu}$ $= K_{c1} \cdot R_1 \cdot [\varepsilon_{T1} + \varepsilon_{ca}(3)] + K_{c2} \cdot R_2$ $\cdot [\varepsilon_{T2} + \varepsilon_{ca}(28) - \varepsilon_{ca}(3)] + K_{c2} \cdot R_3 \cdot \varepsilon_{cd} - 0.5\varepsilon_{ctu}$ where $\varepsilon_{ctu}(t) = \frac{f_{ct,0.05}(t)}{E_{cm}(t) \cdot K_c}$	$w_{max} = s_{r,max} \cdot (\varepsilon_{sm} - \varepsilon_{cm})$
EN 1992-1-1:2023	$s_{rm} = 1.5 \cdot c + \frac{k_{f1} \cdot k_b}{7.2} \cdot \frac{\phi}{\rho_{eff}} \leq \frac{1.3}{k_w} (h - x)$ $k_w = 1.7$	$\varepsilon_{cr} = \varepsilon_{rest} - k_t \cdot \varepsilon_{ctu} = R_{ax} \cdot \varepsilon_{imp} - k_t \cdot \varepsilon_{ctu}$ $= R_{ax,1} \cdot [\varepsilon_{T1} + \varepsilon_{ca}(t)] + R_{ax,2} \cdot \varepsilon_{T2} + R_{ax,3} \cdot \varepsilon_{cd}(t) - k_t \varepsilon_{ctu}$ where $\varepsilon_{ctu}(t) = \frac{f_{ctm}(t)}{E_{cm}(t)}$ and $k_t = 0.6$	$w_{max} = k_w \cdot s_{rm} \cdot (\varepsilon_{cm} - \varepsilon_{sm})$ $= s_{r,max} \cdot (\varepsilon_{sm} - \varepsilon_{cm})$
CIA Z7/06	$s_{r,max} = 3.4 \cdot c + 0.425 \cdot k_1 \cdot k_2 \cdot \frac{\phi}{\rho_{eff}}$ $k_1 = 1.14$ for good bond	$\varepsilon_{cr} = \varepsilon_{rest} - \varepsilon_{ctu} = R \cdot \varepsilon_{imp} - \varepsilon_{ctu}$ where $\varepsilon_{rest} = \sigma_{cs}/E_{c,eff}$ and $R = \varepsilon_{rest}/\varepsilon_{imp}$	$w_{max} = s_{r,max} \cdot (\varepsilon_{sm} - \varepsilon_{cm})$
AIJ-SRC	transfer length: $2l_e = 0.1 \frac{\phi}{\rho}$ crack spacing: $s_{rm} = \frac{l}{m} \geq 2l_e$ where $m = 1 + \frac{L \cdot \alpha_e \cdot \rho}{2 \cdot l_e} \cdot \left(\frac{R \cdot \varepsilon_{imp} - \varepsilon_{ctu}}{b \cdot \varepsilon_{ctu}} \right)$	not determined explicitly ε_{imp} is limited to drying and autogenous shrinkage	$w_{mean} = 2l_e \left(\frac{\sigma_s}{E_s} + \frac{R \cdot \varepsilon_{imp}}{b} \right)$ R represents the actual degree of restraint in a wall
ACI 207.2 & 224	$s_{r,max} = \frac{w}{1.5 \cdot (R \cdot \varepsilon_{imp} - \varepsilon_{ctu})}$ based on the known crack width	$\varepsilon_{cr} = \varepsilon_{rest} - \varepsilon_{ctu} = R \cdot \varepsilon_{imp} - \varepsilon_{ctu}$	$w_{max} = 0.0145 \cdot \sigma_s \cdot \sqrt[3]{a_s \cdot A_{c,eff}} \cdot 10^{-3}$

where:		R	restraint factor (from linear analysis)
a_s	distance from tensioned edge of section to centre of gravity of reinforcement	R_{ax}	restraint factor accounting for creep
c	concrete cover	α_e	ratio of moduli of elasticity of steel and concrete
f_{ct}	tensile strength of concrete	ρ	reinforcement ratio
$f_{ctk,0.05}$	5%-quantile characteristic tensile strength of concrete	ρ_{eff}	effective reinforcement ratio
f_{ctm}	mean tensile strength of concrete	σ_s	stress in reinforcement
k_i	coefficients	ϵ_{ca}	autogenous shrinkage strain
l_e	transfer length	ϵ_{cd}	drying shrinkage strain
s_0	slip length, $s_0 = 2l_e$	ϵ_{cm}	mean strain in concrete
s_{rm}	mean crack spacing	ϵ_{cr}	crack-inducing strain in edge-restrained element
$s_{r,max}$	maximum crack spacing	ϵ_{ctu}	tensile capacity of concrete
w_{mean}	mean crack width	ϵ_{free}	free (unrestrained) part of imposed strain
w_{max}	maximum crack width	ϵ_{imp}	imposed strain (thermal, shrinkage)
$A_{c,eff}$	effective tensile area of concrete	ϵ_{rest}	restrained part of imposed strain
$E_{c,eff}$	effective modulus of elasticity of concrete	ϵ_{sm}	mean strain in reinforcement
E_s	modulus of elasticity of steel	ϵ_T	thermal strain
K_c	coefficient taking into account the effect of creep	ϕ	diameter of reinforcement

3 Demonstration example

3.1 Data

The case is a concrete wall cast on a rigid foundation. A schematic diagram of the investigated case is shown in Fig. 2 while Table 3 enlists the data assumed for the analysis.

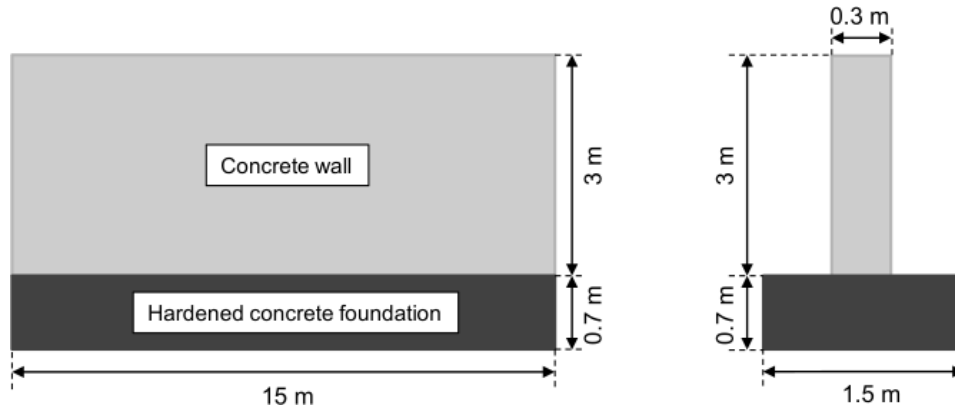


Figure 2. Layout of the hypothetical case study for a wall cast on rigid foundation.

Table 3. Input parameters for cracking models for a demonstration example.

Limit surface crack width [mm]	0.3
Strength class according to EN 1992-1-1:2004 [5]	C30/37
Cement type according to EN 206 [30]	CEM II 32.5R
Characteristic compressive strength of concrete f_{ck} [MPa]	30
Yield strength of reinforcing steel f_{yk} [MPa]	500
Elastic modulus of reinforcing steel E_s [GPa]	200
Thermal dilation coefficient of concrete and steel [$\mu\epsilon/^\circ\text{C}$]	10
Cover to reinforcement [mm]	40
Early-age temperature drop [$^\circ\text{C}$]	20
Long-term temperature change [$^\circ\text{C}$]	20
Total free autogenous shrinkage [$\mu\epsilon$] $\epsilon_{ca,\infty}$	50
Total free drying shrinkage [$\mu\epsilon$] $\epsilon_{cd,\infty}$	300

It was assumed that both the wall and foundation were made of the same C30/37 class concrete, with the characteristic compressive strength of 30 MPa according to EN 1992-1-1:2004 [5] which value was used for calculations with all the methods. The concrete mix was assumed to be composed of CEM II 32.5R cement and natural quartzite aggregate. This type of cement was classified as “ordinary” cement

according to the AIJ-SRC recommendations [16] and as “Type I” cement according to the ACI Report 209 [31]. The analysed wall was cast 28 days after the foundation and it was assumed that at the time of casting of the wall the concrete of the foundation has achieved its mature properties.

All the values of imposed deformations were estimated with CIRIA C766 [15] to provide realistic values representative for the analysed case. To maintain consistency throughout the methods, the age of concrete for the early-age analysis was taken as 3 days. The autogenous shrinkage strain at after 3 days was taken as $15 \mu\epsilon$ following EN 1992-1-1:2004 [5]. The drying shrinkage was taken as uniform in the cross-section (a mean value of $300 \mu\epsilon$) and the effect of self-equilibrating stresses induced by the actual variation of shrinkage in the cross-section were taken into account indirectly, if allowed for in a model.

3.2 Results and discussion

In the first step, the crack width was calculated for given reinforcement. The applied reinforcement ($\phi 12$ bars spaced by 160 mm placed symmetrically at both sides of the wall; reinforcement ratio of 0.47%) was determined with the method of EN 1992-1-1:2004 & EN 1992-3:2006 to limit the final width of the crack to $w_{lim} = 0.3$ mm. Figure 3 shows comparison between the crack width obtained with each method for this reinforcement. Detailed intermediate results are listed in Table 4. In the second step of calculations, each method was used to calculate the reinforcement required to limit the final crack width to $w_{lim} = 0.2$ mm, 0.3 mm and 0.4 mm. The results are presented in Fig. 4.

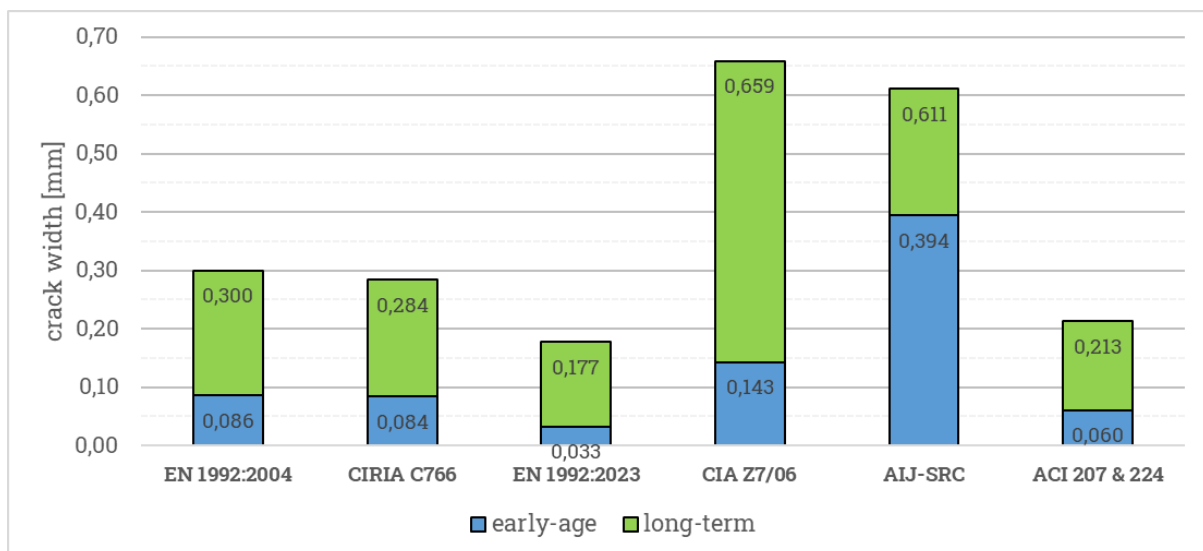


Figure 3. Comparison between crack width estimations in a demonstration example of a wall for given reinforcement ($\phi 12$ cc 160 mm) with different standardised methods.

Table 4. Details of crack width calculations for a demonstration example with different standardised methods.

property	EN 1992-1-1:2004 & EN 1992-3:2006	CIRIA C766	EN 1992-1-1:2023	CIA Z7	AIJ-SRC	ACI 207.2 & 224
$A_{c,eff}$ [cm ²]	1150	1150	1060	1500	1500	1500
ρ_{eff} [%]	0.61	0.61	0.67	0.47	0.47	0.47
EARLY-AGE CRACK WIDTH						
$f_{ct}(3)$ [MPa]	1.73	1.21	1.46	1.11	n/a	1.20
$E_c(3)$ [GPa]	27.4	27.4	21.9	20.1	20.4	17.5
φ_{ea}	0.55	0.54	0.55	0.55	0.55	n/a
$E_{c,eff}(3)$ [GPa]	17.7	17.8	14.1	13	13.2	17.5
ε_{imp-ea} [με]	214.6	214.6	194.6	214.6	214.6	214.6
ε_{ctu-ea} [με]	63.3	68.1	66.8	55.2	75.1	100.0
$s_{r,max-ea}$ [cm]	80.0	108.4	56.9	137.3	375**	256.3***
R at early age	0.50*	0.80	0.50*	0.74	0.80	0.63
$\varepsilon_{rest-ea}$ [με]	107.3	111.6	97.3	159.0	n/a	135.8
ε_{cr-ea} [με]		77.6	57.2	103.8		35.8
w_{ea} [mm]	0.086	0.084	0.033	0.143	0.394	0.060
LONG-TERM CRACK WIDTH						
$f_{ct}(\infty)$ [MPa]	2.9	2.03	2.9	1.97	n/a	2.73
$E_c(\infty)$ [GPa]	32	32	32	29.6	25.3	25.9
φ_{lt}	1	1	1	1	1	n/a
$E_{c,eff}(\infty)$ [GPa]	16	16	16	14.8	12.6	25.9
ε_{imp-lt} [με]	750.0	750.0	730.0	750.0	750.0	750.0
ε_{ctu-lt} [με]	90.6	126.9	90.6	66.7	114.8	150.0
$s_{r,max-lt}$ [cm]	80.0	108.4	56.9	137.3	136.4**	55.8***
R in long term	0.50*	0.80	0.50*	0.73	0.80	0.54
		0.80	0.50*			
$\varepsilon_{rest-lt}$ [με]	375.0	325.8	365.0	546.4	n/a	403.8
ε_{cr-lt} [με]		262.3	310.6	479.4		253.8
w_{lt} [mm]	0.300	0.284	0.177	0.659	0.611	0.213

* accounts for creep

** mean crack spacing (in crack-formation phase) to be multiplied by 1.7 to convert w_{mean} to w_{max}

*** calculated from the crack width

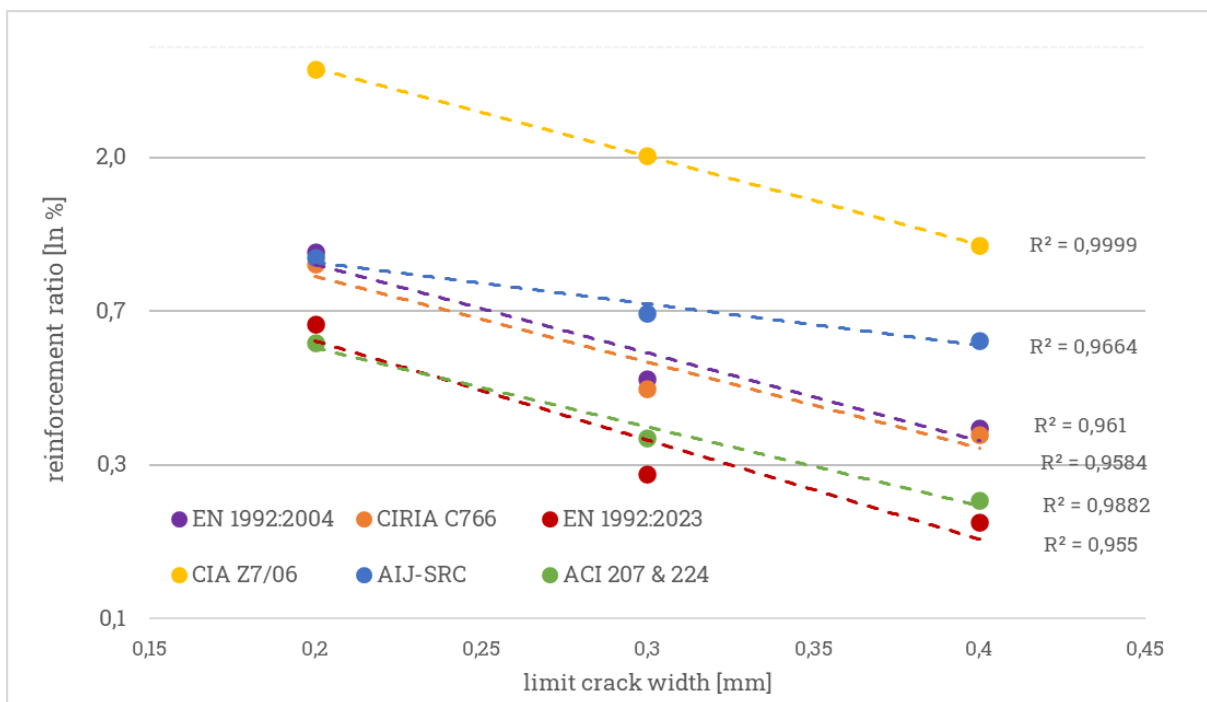
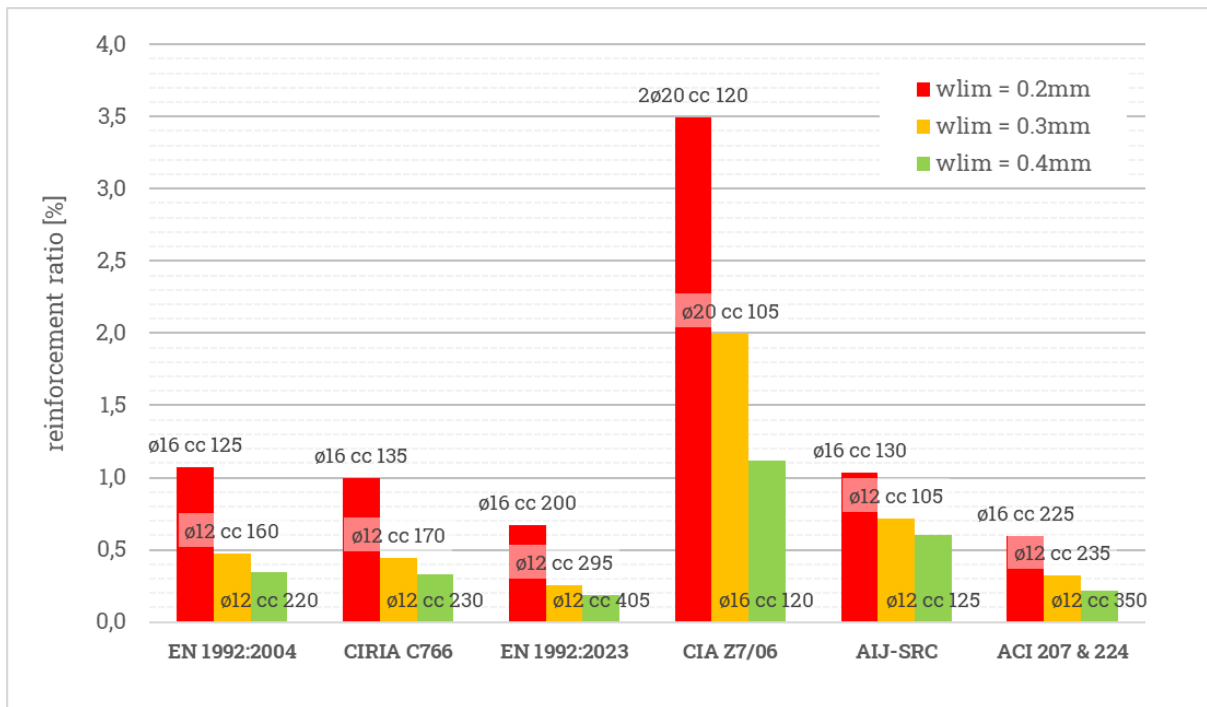


Figure 4. Comparison between reinforcement required to limit the long-term (final) crack width in a demonstration example with different standardised methods.

3.2.1 EN 1992-1-1 and related documents

Comparing the European methods, i.e. past version of EN 1992-1-1:2004 [5] and EN 1992-3:2006 [6], CIRIA C766 [15] and new version of EN 1992-1-1:2023 [14], it can be observed that for the same applied reinforcement the obtained width of the crack decreases (Fig. 3). Naturally, analogical

observation can be made when comparing the reinforcement ratios required to limit the crack widths (Fig. 4). For each analysed scenario the greatest area of the required reinforcement is predicted by EN 1992-1-1:2004 & EN 1992-3:2006 method, followed by the CIRIA C766 and then EN 1992-1-1:2023 approaches. One may infer that the guidelines of CIRIA C766 and EN 1992-1-1:2023 by proposing modifications to the method of EN 1992-1-1:2004 & EN 1992-3:2006 aim at providing more economical and sustainable design solutions. This is predominantly attributed to the lower value of the crack-inducing strain, which in case of CIRIA C766 and EN 1992-1-1:2023 takes into account concrete extensibility (strain relief) after cracking (see Table 4).

The predicted value of the crack-inducing strain is higher at early-age (77.6 vs. 57.2 $\mu\epsilon$) but lower in long-term (262.3 vs. 310.6 $\mu\epsilon$) with the method of CIRIA C766 in comparison to EN 1992-1-1:2023. Although the methods of CIRIA C766 and EN 1992-1-1:2023 use the same philosophy for determination of this strain, there are two important factors responsible for the difference. First, in EN 1992-1-1:2023 the effect of creep on the reduction of stresses is already accounted for in the value of the degree of restraint, and by default there is no differentiation proposed to be made between its early-age ($R_{ax,1}$) and long-term ($R_{ax,2}$ and $R_{ax,3}$) values. In the early-age analysis the default recommended values of the restraint factors according to both methods are almost equal (0.5 in EN 1992-1-1:2023 vs. $0.8 \cdot 0.65 = 0.52$ in CIRIA C766). The free strain, however, is lower by EN 1992-1-1:2023 (194.6 vs. 214.6 $\mu\epsilon$ in CIRIA C766) as the standard allows for the reduction of the early-age thermal strain to account for the positive effect of compressive stresses in heating phase ($0.9\epsilon_{T1}$). In the long-term analysis, in turn, the effective restraint factor by CIRIA C766 is lower ($0.8 \cdot 0.5 = 0.4$ in comparison to 0.5 by EN 1992-1-1:2023) due to the higher effect of creep, thus the restrained part of strain is also lower.

A comment must be made, however, about the restraint factor value used in the calculations. Numerous discussions have been made, also by the authors [1, 12], about the challenges in determination of the decisive degree of restraint for crack width calculations in wall-on-slab structures. In this study default values proposed by the standards were used. However, some of the guidelines provide detailed recommendations for more precise calculation of the degree of restraint. CIRIA C766 refers in this regard to the proposal of ACI 207 to calculate the axial restraint factor as:

$$R = \frac{1}{1 + \frac{A_c E_c}{A_F E_F}} \quad (3)$$

The value of the restraint factor calculated with this proposal gives by far the lowest values (0.63 and 0.54 at early-age and long-term, respectively – see Table 4), yet it is the maximum value at the wall–foundation joint, while the decisive location where the maximum crack width is expected lies somewhere above the joint. CIRIA C766 suggests this level to be $0.1L$, for which the expected restraint factor at given height h calculated following CIRIA C766 recommendations:

$$R(h) = R \cdot \left[\left(1.372 \cdot \left(\frac{h}{L} \right)^2 - 2.543 \cdot \frac{h}{L} + 1 \right) + 0.044 \cdot \left(\frac{L}{H} - 1.969 \right) \cdot \left(\frac{h}{H} \right)^{1.349} \right] \quad (4)$$

would be even lower, 0.51 and 0.44 at early-age and in long term, respectively.

EN 1992-1-1:2023 also allows for more sophisticated methods to be used, e.g. by determining the degree of restraint through (linear) finite element analysis; the restraint factor could be then calculated acc. to the Eq. (2). EN 1992-1-1:2023. Such an approach seems reasonable especially in case of geometrically complex structures for which simplified methods of determination of the restraint factor cannot be applied. In this regard, the authors refer the reader to the RILEM TC 287-CCS recommendations **Erreur ! Source du renvoi introuvable.** for detailed explanation of FEM-based modelling of structures subjected to imposed strains. For the structures with simpler geometries, such as the ones analysed in the paper, guidance of other standards or recommendations can be used. Such provisions are given, as already mentioned, by ACI 207.2 and CIRIA C766, but also non-standardised solutions exists, which have been discussed in e.g. [32]. Creep relaxation can be also accounted for independently in accordance with Annex D; the influence of concrete age and creep on stress values is taken into account by the effective elastic modulus of concrete, i.e. simplified viscoelastic model.

Secondly, CIRIA C766 accounts additionally for higher level of strain relief ($k_t \varepsilon_{ctu}$ component) in long term than EN 1992-1-1:2023 (63.4 vs. 54.4 $\mu\epsilon$). CIRIA C766 increases tensile capacity of concrete under sustained loading by accounting for the effect of creep (which is not done in EN 1992-1-1:2004 and EN 1992-1-1:2023, where tensile capacity is determined under the assumption of the short-term character of the load – see Table 4). Even though the tensile capacity of concrete according to CIRIA C766 is calculated using the characteristic tensile strength $f_{ct,0.05}$, the age-adjusted modulus of

elasticity of concrete $E_{c,eff}$ is applied. The level of increase is by 8% at early-age and by 40% at long-term in comparison to the scenario in which mean tensile strength and modulus of elasticity are considered.

However, even though the crack-inducing strain is the lowest according to CIRIA C766, the final width of the crack is the lowest based on EN 1992-1-1:2023. This results, in turn, from the crack spacing which is estimated to be twice the value of EN 1992-1-1:2023 by CIRIA C766 (108 vs. 57 cm). In tensioned elements, as the ones studied in this paper, for the same geometry and reinforcement, the crack spacing calculated with the formula of EN 1992-1-1:2023 gives lower values than by the past version of EN 1992-1-1:2004 due to, among the others, reduced impact of concrete cover and favourable effects of bond (coefficient k_1 takes the value of ~0.55 in EN 1992-1-1:2023 in comparison to 0.8 acc. to EN 1992-1-1:2004). CIRIA C766, however, states that the bond properties at early-age are poor and recommends that the value of k_1 should be increased ($k_1 = 0.8/70\% = 1.14$).

If the three methods (of EN 1992-1-1:2004 & 1992-3:206, CIRIA C766 and EN 1992-1-1:2023) were consistent in their assumptions of relevant parameters, i.e. if the value of the modulus of elasticity was reduced by creep and by assuming poor bond between the steel and reinforcement ($k_1 = 1.14$), the observed tendency when comparing the methods would be further enforced. The predicted final width of the crack would be respectively equal to 0.325 mm (EN 1992-1-1:2004 & 1992-3:2006), 0.284 mm (CIRIA C766) and 0.159 mm (EN 1992-1-1:2023).

3.2.2 CIA Z7/06 recommendations

The method of CIA Z7/06 [16] gives by far the greatest width of the crack in the wall (its value is over twice the target limit value of 0.3 mm, so the width of the crack predicted by EN 1992-1-1:2004 & 1992-3:2006 – see Fig. 3). This should be attributed to the crack spacing and restrained part of strain. The spacing of the cracks is calculated after CIRIA C766 (i.e. with the formula of EN 1992-1-1:2004 but with poor bond assumption $k_1 = 1.14$, see Table 2). The crack spacing is further increased by decrease in the effective reinforcement ratio: in the method of CIA Z7/06 the effective tensile area of concrete is not limited as in EN 1992-1-1:2004, but the whole tensioned cross-section is considered. Regarding the restrained part of strain, in the method of CIA Z7/06 the restraint factor is calculated

from the geometry and stiffness of the wall and foundation. Therefore, the restraint factor obtained with this method has the meaning of R factor from CIRIA C766 rather than that of R_{ax} from EN 1992-3:2006. Consequently, the effect of strain reduction by creep is not taken into account in this method. Finally, the CIA Z7 methods takes into consideration the effect of strain relief, in contrary to EN 1992-1-1:2004.

If good bond was assumed ($k_1 = 0.8$), the expected widths of the cracks would decrease from 0.143 mm and 0.659 mm (see Fig. 3) to 0.104 mm and 0.481 mm (i.e. by 27%) for early-age and long-term, respectively. Furthermore, if the tensile area was further reduced according to the recommendations of EN 1992-1-1:2004 to the effective area $A_{c,eff}$ (from 1500 to 1150 cm²), the resultant widths of the cracks would be reduced to 0.083 mm and 0.384 mm (i.e. by 42%), respectively. It must be noted that the analysed element is relatively thin, so the range of impact of the reinforcement is high ($h_{c,eff}$ by EN 1992-1-1:2004 is 77% of $0.5h$). Thus, with an increasing thickness of the element the influence of the effective reinforcement ratio would be increasing. Finally, if the value of the restraint factors R calculated with the method of CIA Z7/06 were reduced from 0.74 and 0.73 to 0.5 for early-age and 0.4 for long-term (to account for the reduction by creep as in EN 1992-1-1:2004 and CIRIA C766), the resultant crack width would be reduced to 0.042 mm and 0.187 mm (i.e. by 72%), respectively.

3.2.3 AIJ-SRC recommendations

A comparably large final crack width was obtained with the AIJ-SRC method [16] (0.611 mm for a long-term crack width – see Fig. 3), in addition to the fact that with this method the greatest early-age crack width was predicted (0.394 mm). This method was derived from different assumptions than the previous ones. First, it does not assume the stabilised crack spacing being reached. Therefore, the calculated transfer length $s_0 = 2l_e$ is compared with the calculated crack spacing s_r , as it is expected that in the crack-formation stage s_0 is smaller than the actual spacing of the cracks (this assumption has been proven true in the course of calculations). Secondly, uniform spacing between the cracks is considered when determining the stress in reinforcement, so the resultant width of the crack is a mean width. For the sole purpose of this comparative study the crack widths obtained with the use of this method were multiplied by 1.7 to convert them to the maximum values.

It is interesting to notice that according to the AIJ-SRC method the early-age crack width increases by only 50% in long term (from 0.39 mm to 0.61 mm – see Fig. 3) while the strain is more than tripled (free strain increases from 215 $\mu\epsilon$ to 750 $\mu\epsilon$ – see Table 4). This is opposite to the results of other methods in which the crack width increase corresponds to the increase in strain. It is also worth mentioning the amount of reinforcement required to limit the crack width according to AIJ-SRC method in comparison to the CIA Z7/06 approach, which predicted comparably high widths of the crack. With a comparable expected crack width of ~0.6 mm, it is enough to increase the reinforcement area by 50% to reduce the crack width by half, while it must be increased 4 times to achieve the same effect according to CIA Z7/06 (see Fig. 4). In general, the reinforcement requirements evaluated with the CIA Z7/06 approach are the highest for all the analysed limit crack widths. It is also interesting to notice that the decrease in the required reinforcement with an increasing limit crack width predicted with CIA Z7/06 is practically linear while for all other methods the differences become smaller (reduction by ~half between 0.2 mm and 0.3 mm, and reduction by ~quarter between 0.3 mm and 0.4 mm, as can be seen in Fig. 4).

It must be emphasised that the method of AIJ-SRC modifies the original Base–Murray method [26] derived from the model of a fixed tie (100% degree of restraint) by introduction of the restraint factor to account for the partial restraint in the wall. However, it can be observed that the model is almost insensitive to the degree of restraint (thus the restrained part of strain) until the stabilised crack spacing is reached: increase in strain causes formation of new cracks, not the increase of the crack width. First crack is predicted to be formed for the restraint factor of 0.2; by increasing the restraint factor up to 1, the predicted number of cracks increases from 1 to 5 at early age and from 2 to 14 in long term, while the change in the crack width is as little as from 0.36 mm to 0.42 and from 0.57 to 0.65, respectively.

3.2.4 ACI reports 207.2 and 224

In the method proposed in the ACI reports the maximum crack spacing is obtained from the mean spacing with the conversion factor of 1.5 instead of 1.7. This procedure accounts also for the restraining moment and its effect on the width of the crack. It must be emphasised that according to the approach of the ACI reports the effect of creep is negligible, so the calculation procedure is based on the linear elastic analysis.

The ACI 207.2 report [18] provides a method to determine the value of the restraint factor taking into account the relative stiffness of the wall and foundation. It must be noted that the time-development of the modulus of elasticity according to the ACI report [31] is significantly slower than according to other methods, e.g. EN 1992-1-1:2004 [5], thus for the early-age analysis (after 3 days) the ratio between the early-age and 28-days moduli is ~ 0.7 in comparison to ~ 0.9 for EN 1992-1-1:2004. The obtained values of the restraint factor are visibly smaller than those obtained with the method of CIA Z7/06 (0.63 vs. 0.74 and 0.54 vs. 0.73 at early age and long term, respectively), and the highest value recommended by CIRIA C766 (0.8) – see Table 4.

Additionally, the level of extensibility (strain relief related to tensile capacity of concrete) recommended by ACI 207.2 report [18] is relatively high: $100\ \mu\epsilon$ at early age and $150\ \mu\epsilon$ in long term are the highest values of all the methods. According to other methods, the tensile strain capacity can be calculated as a ratio between the tensile strength and modulus of elasticity. If the tensile strain capacity was calculated like that for the actual values of these mechanical properties as recommended by the ACI report, they would be smaller: $\epsilon_{ctu} = f_{ct}/E_c = 71.2\ \mu\epsilon$ and $105.3\ \mu\epsilon$ for early-age and long-term. Consequently, the early-age and long-term crack widths would increase from 0.060 mm and 0.213 mm (see Fig. 3) to 0.080 mm and 0.222 mm (by 33% and 4%), respectively. Finally, if the same value of the mean-to-maximum crack width conversion factor ($\beta = 1.7$ instead of 1.5) was taken, these crack widths would further increase to 0.084 mm and 0.229 mm (increase by 40% and 8%, respectively). These would still be, however, one of the lowest predictions of crack widths obtained with the analysed methods.

The required reinforcement ratios predicted with the ACI method is comparable with the predictions of the EN 1992-1-1:2023; these two methods give the lowest required reinforcement ratios to limit the crack widths (see Fig. 4). In the ACI approach this should be attributed to the positive effect of the restraining along the edge of the wall which together with the reinforcement guarantees a sufficient restraining moment, ensuring formation of a suitable number of cracks and by that reducing their widths. A general comment can be made when analysing Fig. 4b about the effectiveness of the reinforcement to limit the crack width. It can be concluded that all the methods reproduce the real-life observation made by the authors in [1] that with increasing reinforcement ratio the effectiveness in crack with

limitation decreases, i.e. the reinforcement requirements increase exponentially with a decrease of the limit crack width.

4 Case study 1: Massive wall of Civaux NPP mock-up

4.1 Description of the structure

The analysed wall was an experimental mock-up nuclear containment wall for a newly constructed nuclear power plant near Civaux, France, which can be classified as massive according to [34]. Figure 5 schematically shows the geometry and cracking pattern in the wall. The data of the analysed case study are retrieved from the works [35], [36], [37], [38] and [39], and are presented in detail in Appendix A, sec. A.1. In the following sections the crack width calculations with the use of the studied methods are performed, and include comparison between the crack spacing, crack-inducing strain and predicted crack width.

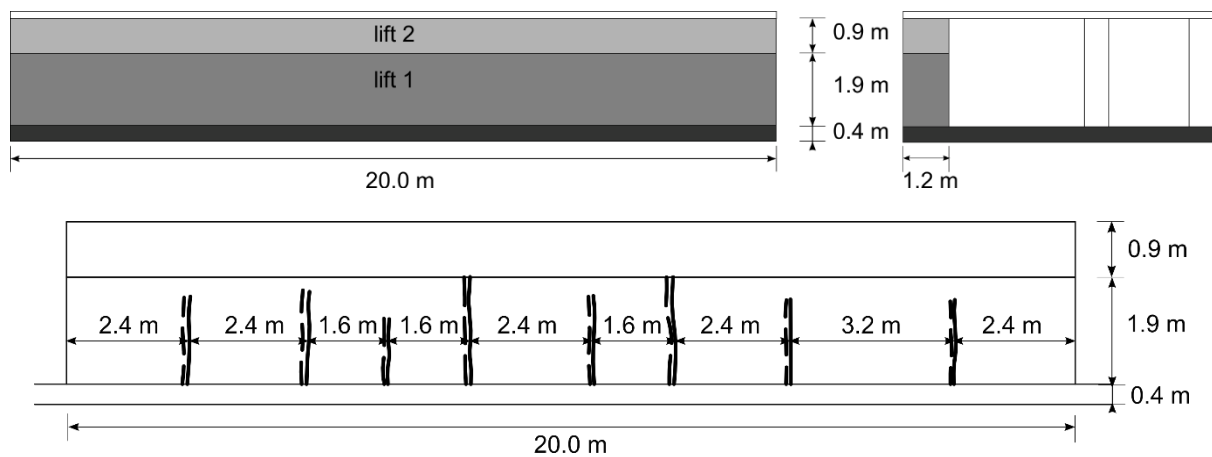


Figure 5. Civaux mock-up wall: longitudinal view; cross-section; cracking pattern (crack widths 1×0.04 mm, 4×0.1 mm, 2×0.2 mm and 1×0.5 mm).

4.2 Estimate of crack-inducing strain

Calculation of the crack-inducing strain requires determination of three components (see Table 2): (1) magnitude of imposed deformation induced by temperature variation and shrinkage ε_{imp} , (2) degree of restraint R and (3) tensile capacity ε_{ctu} . In the analysed case the cracking was caused by temperature variations due to simultaneous heating up of hardening concrete and its cooling to the ambient temperature, as well as autogenous shrinkage. As the wall was kept in formwork over the period of cooling, it could be assumed that drying was negligible.

454 Thermal strain was calculated as a product of temperature difference and coefficient of thermal dilation
 455 of concrete $\varepsilon_T = \alpha_T \cdot \Delta T$. Some of the analysed standards give recommendations how the temperature
 456 difference ΔT should be determined. According to CIRIA C766 [15] and ACI 207.2 [8] the temperature
 457 drop should be calculated as the difference between the maximum (peak) temperature and ambient
 458 temperature: $\Delta T = T_{\max} - T_a$. This means that the design thermal strain accounts for the whole
 459 temperature drop during cooling. EN 1992-1-1:2023 [14], in turn, recommends that the thermal strain
 460 responsible for cracking should be determined at the critical time t_{crit} which is the time instant when
 461 cracking is likely to occur, and as a difference between the peak temperature and the temperature of the
 462 restraining element at that time: $\Delta T = T_{\max} - T_0$. If no better data is available, the latter one can be
 463 assumed as the ambient temperature, however, in the case of a wall-on-slab structure the actual
 464 temperature of the restraining element (foundation) can be higher due to its re-heating by the hardening
 465 wall. Furthermore, EN 1992-1-1:2023 accounts also for the fact that initial heating of the wall induces
 466 positive compressive stresses which reduce the value of the proceeding tensile stresses during cooling.
 467 Consequently, the standard recommends reducing the design thermal strain by the factor $k_T = 0.9$.
 468 The above-mentioned provisions consider maximum mid-span, mid-section temperature, so the
 469 maximum possible temperature in the whole wall over the whole period of concrete hardening. In case
 470 of the elements with relatively low massivity, which are characterised by small variations of
 471 temperature in the cross-section, this assumption is correct. The challenge arises in more massive
 472 elements, such as the analysed wall, in which the cross-sectional temperature variation is non-
 473 negligible. Given the risk of through cracking, confirmed in the observations of the actual wall, it may,
 474 hence, seem reasonable to consider in the calculations the thermal strain which gives zero self-induced
 475 stress (the strain on the so-called compensation line – see Fig. 6). CIRIA C766 [15] recommends in
 476 such a situation to use the mean temperature in the cross-section which – assuming parabolic
 477 distribution of temperature in the cross-section – can be calculated as $T_{\text{mean}} = T_{\text{int}} - \frac{1}{3}(T_{\text{int}} - T_{\text{sur}})$.
 478 Given the above considerations, the input data taken for further calculations were collectively presented
 479 in Table 5. When analysing the diagram of temperature development in the wall (Fig. A.4) it can be
 480 seen that over the period when measurements were recorded – until the time of formwork removal – no

temperature equalisation was reached while the wall had already cracked. The exact time of cracking is, however, not known. Therefore, following the recommendations of CIRIA C766, the analysis was performed at the time t_{crit} of 3 days.

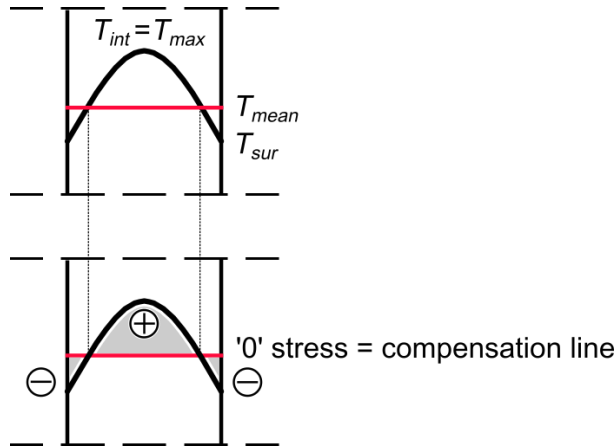


Figure 6. Method for determination of temperature for calculation of design early-age thermal strain.

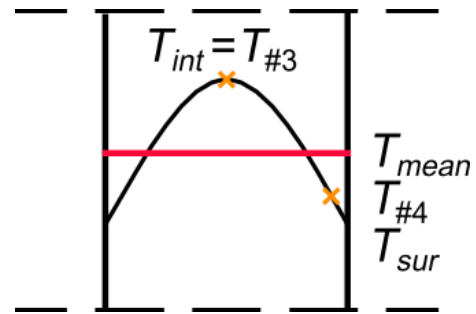


Figure 7. Mean temperature in the Civaux mock-up wall.

The temperature difference was calculated as the difference between the mean temperature in the cross section at the time of the peak temperature occurrence and the temperature of the foundation at t_{crit} . The peak temperature was the maximum temperature measured by thermocouple #3 located in the core of the wall while the surface temperature was calculated based on the measurements of thermocouples #3 and #4 (see Fig. 7). Temperature difference in the cross-section was equal to $\sim 9^{\circ}\text{C}$. The T_0 temperature was taken from the measurements of thermocouple #1, which was located in the raft foundation just below the wall (see Fig. A.3). It can be observed that after re-heating to the temperature of $\sim 24^{\circ}\text{C}$, the raft cooled down steadily and after 5 days (up to when the measurements were available) it reached 20°C ; after 3 days its temperature was still around the peak value of 24°C (see Fig. A.4).

Table 5. Calculation of thermal strain 3 days after casting of the first lift in the Civaux mock-up wall.

T_{max} [$^{\circ}\text{C}$]	59.3
T_{sur} [$^{\circ}\text{C}$]	50.2
T_{mean} [$^{\circ}\text{C}$]	56.3
T_a [$^{\circ}\text{C}$] – mean	11.4
T_0 [$^{\circ}\text{C}$]	24

$\Delta T = T_{\text{mean}} - T_0 \text{ [}^\circ\text{C]}$	32.3
$\varepsilon_T = \alpha_T \cdot (T_{\text{mean}} - T_0)$	323 $\mu\varepsilon$

It should be mentioned that time-development of concrete's properties is related to the progress of its maturity, which is a temperature-dependent phenomenon. In case of massive structures, such as the analysed wall, in which significant increase of temperature is observed over long period, these processes develop visibly faster. Therefore, the equivalent age of concrete, not the real one, should be used for determination of these values at the time of analysis. Normally, determination of the equivalent age is difficult at the design stage when temperature history is not known. However, for the specific case of the Civaux wall, the equivalent age of concrete, calculated according to EN 1992-1-1:2004 [5], at the age of 3 days was approximately 10 days (calculated based on the mean temperature in the cross-section), which is an important difference.

The value of the autogenous shrinkage strain was calculated using the laboratory test results presented in Fig. A.5 with the EN 1992-1-1:2004 [5] model and least-square method approximation. At the time $t_{\text{crit},eq} = 10$ days the autogenous shrinkage was estimated to be 30.3 $\mu\varepsilon$.

The compressive strength and modulus of elasticity were measured only since the 28th day. For early-age analysis the measured 28th-day values were taken as a basis and the values of tensile strength and modulus of elasticity at time $t_{\text{crit},eq}$ were calculated following each considered method. Figure 8 presents a comparison between the values obtained with these methods. It must be emphasised that the CIA Z7/06 recommends fixed values of early-age tensile strength and modulus of elasticity for a 3-day old concrete, which is a sensible value as long as the actual age and equivalent of this concrete comply. For a massive structure such as the analysed one these recommendations are not valid.

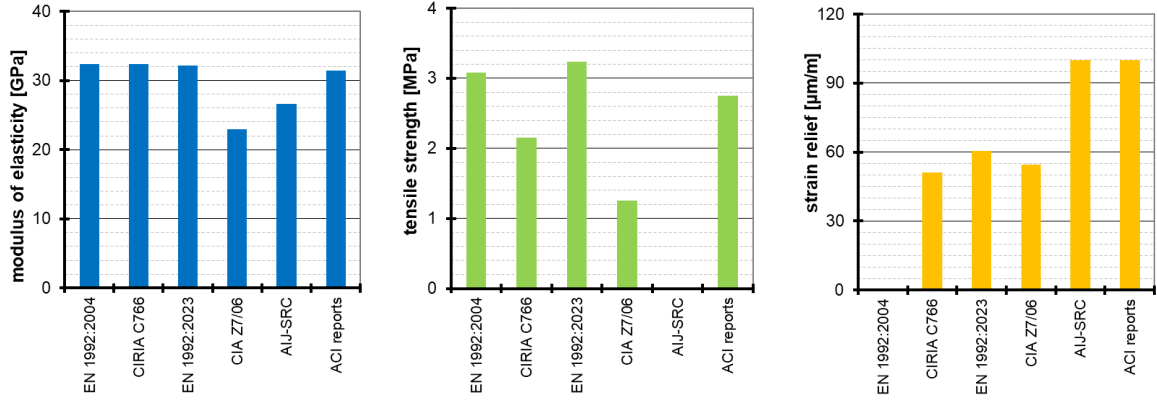


Figure 8. Mechanical properties of the Civaux wall concrete after 3 days (10 days of equivalent age) assessed with different design methods.

Finally, to calculate the crack-inducing strain, the restrained part of imposed strain must be determined, which deems to know the degree of restraint (expressed with the restraint factor). Regarding the restraint factor, EN 1992-3 [6] recommends the maximum, default base restraint factor of 0.5 (which accounts for creep) while CIRIA C766 [15] recommends the default value of 0.8 (without considering creep). Alternatively, CIRIA C766 refers to the formula proposed by ACI 207.2 [8] given by Eq. (3), which according to Eq. (4) depends on the L/H ratio of the restrained element, and for the Civaux wall with $L/H \geq 10$ it is constant over the height. The relative stiffness of the wall depends, in turn, on the geometry of the wall and foundation A_c/A_F , which stay unchanged over the analysed period, and their moduli of elasticity E_c/E_F , which evolve in time. The restraint in this case is not typical, as it is in a form of a raft foundation. Following the recommendations of ACI 207.2 [8] in such a case it can be assumed that $A_c/A_F = 2.5$. The resultant restraint factor depends therefore on the applied time-development function of the modulus of elasticity which determines the E_c/E_F ratio, and differs among the methods only slightly from 0.72 to 0.73 (in elastic analysis). Finally, the restraint factor estimated with CIA Z7 [16] method in elastic analysis is equal to 0.82 (see Table 6), but it should be noted that CIA Z7 assumes the slowest development of the modulus of elasticity of all the methods (see Fig. 8b). Given the above, the restraint factor $R = 0.8$ was assumed for calculations as a safe estimate in all the methods where no specific recommendations were given. The effect of creep on partial relief of restrained strains was accounted for by reducing the value of the degree of restraint by factor $K_c =$

1/(1 + φ) equal to 0.65 following CIRIA C766. The resultant restrained part of strain and crack-inducing strains are collectively presented in Table 6.

Table 6. Calculation of crack-inducing strain 3 days after casting of the first lift in the Civaux mock-up wall.

	EN 1992-1-1 :2004 & 1992-3:2006	CIRIA C766	EN 1992-1- 1:2023	CIA Z7/06	AIJ-SRC	ACI 207.2
Thermal strain ε_T	323 (from Table 5)					
Autogenous strain ε_{ca}	30.3					
Imposed strain ε_{imp}	353.3					
Restraint factor R	0.5 (creep)	0.8 (no creep) $K_c = 0.65$	0.5 (creep)	0.82 (no creep)	0.8 (no creep) $K_c = 0.65$	0.8 (no creep)
Restrained strain ε_{rest}	176.6	183.7	176.6	288.3	n/a	282.6
Crack-inducing strain $\varepsilon_{cr} =$ $\varepsilon_{rest} - k_t \varepsilon_{rctu}$	176.6	132.5	116.2	233.8	n/a	182.6

Table 6 collects also the predictions of the crack-inducing strain in the analysed wall calculated with different methods. The same value of the total free strain was assumed. The differences in the restrained strain result mainly from the differences in the assumed value of the restraint factor, while in the case of the crack-inducing strain further from the difference in the magnitude of the assumed strain relief (extensibility). Consequently, the lowest value of the crack-inducing strain is predicted with EN 1992-1-1:2023, then CIRIA C766 and EN 1992-1-1:2004 & EN 1992-3:2006, with comparable prediction of ACI 207.2 & 224, and the highest value is predicted with CIA Z7/06 method. This complies with the tendency defined in Table 4. No direct comparison can be made with the method of AIJ-SRC because of different assumptions of the model in which the crack-inducing strain is not explicitly calculated.

4.3 Crack width

The widths of the cracks predicted with the analysed methods differ significantly, with over triple difference between the extreme values (see Table 7).

Table 7. Calculation of crack width 3 days after casting of the first lift in the Civaux mock-up wall.

	EN 1992-1-1:2004 & EN 1992-3:2006	CIRIA C766	EN 1992-1-1:2003	CIA Z7/06	AIJ-SRC	ACI 207.2 & ACI 224	measured
Calculated slip length $2l_{e,max}$ [m]	0.75	1.00	0.60	1.00	$s_{r,max} = 2.17$ $s_0 = 0.17$	0.91	Max spacing 3.2
w_{max} [mm]	0.133	0.133	0.070	0.235	0.219	0.248	0.2 (0.5*)

* can possibly be treated as an exceptional anomaly

The methods of the current version of EN 1992-1-1:2004 & EN 1992-3:2006, CIRIA C766, EN 1992-1-1:2023 and CIA Z7/06 are easily comparable because they are based on the same model. The differences result first of all from the predicted transfer length over which the strain difference occurs. It must be remembered that in case when the element is in the crack formation stage, the calculated value of $s_{r,max}$ must be understood as twice the transfer length, and evidently all these methods predict this distance to be significantly smaller than the crack spacing. The greatest length of strains incompatibility is predicted with CIRIA C766 (and CIA Z7/06, which uses the same formula) because of the assumption of poor bond properties. The smallest length is predicted with EN 1992-1-1:2023, which in turn less conservatively takes into account the influence of both the bond properties and concrete cover.

The differences in the crack width are further caused by the value of the restraint factor (hence the restrained part of strain) and the level of strain relief. The highest magnitude of the crack-inducing strain is predicted with CIA Z7/06 method in which the restrained strain is determined without taking into account the effect of creep (linear-elastic restraint factor), which consequently results in the greatest predicted crack width. EN 1992-1-1:2023, in turn, predicts the smallest magnitude of crack-inducing strain, mainly due to the highest expected level of strain relief. This, coupled with small crack spacing, results in the smallest predicted crack width. The methods of EN 1992-1-1:2004 and CIRIA C766 give in this case comparable results.

Comparison of the remaining two methods (AIJ-SRC and ACI 207.2 & 224) is more difficult, because they are based on different models. The same value of the restraint factor is taken in both methods. In

the AIJ-SRC approach the effect of creep is taken into account while in the ACI approach neglects the effect of creep. Yet, the obtained width of the cracks are of comparable magnitude and are as large as predicted by the CIA Z7/06 method.

Even though it is not an intention of the standardised methods to compare the calculated crack width with those actually measured on site, it is a common practice to control the compliance of the structure with its design by doing such comparison. This, however, requires understanding of the crack width model assumptions. First of all, cracking is a highly stochastic process, and therefore some margin of error must be accepted. This margin might be related to the difference between the calculated and measured crack width, as discussed in [12]. Another point of view might be in the expected outcome. For instance, if one takes into account possible uncontrollable random effects such as inaccuracies during execution, it might be accepted that individual cracks might exceed the design limits as they can be easily repaired with negligible effect on the integrity of the structure and the budget of the investment.

Given the latter, i.e. if a single crack of 0.5 mm could be treated as an accepted, unique abnormality, the crack widths predicted by the methods of CIA Z7/06, AIJ-SRC and ACI 207.2 & 224 (0.235, 0.219 and 0.248 mm – all greater than 0.2 mm) would be larger in comparison with the measured crack widths. The methods of EN 1992-1-1:2004 & EN 1992-3:2006, CIRIA C766 and EN 1992-1-1:2023, however, in this particular case underestimate the widths of the cracks to an unacceptable level. The characteristic crack width is defined as the width with 5% probability of being exceeded, but even if the margin of error of 20% would be assumed following *Beeby* [40], it would allow some cracks to reach up to 0.16 mm according to EN 1992-1-1:2004 & EN 1992-3:2006 and CIRIA C766, and even as little as 0.085 mm according to EN 1992-1-1:2023. With the maximum crack width of 0.2 mm the level of underestimation is 50% for past EN 1992 and CIRIA C766, and almost 300% for new EN 1992-1-1.

4.4 Minimum reinforcement

A comment should be made on the applied reinforcement with respect to the minimum reinforcement requirements. The applied reinforcement ($\phi 20$ cc 180 mm, $A_s = 17.5 \text{ cm}^2$) would be below the minimum required reinforcement if one would take the tensile area of concrete right before cracking A_{ct} equal to half the cross-section ($A_{s,\min} = 34.3 \text{ cm}^2$ in this case). While this is a good assumption for thin sections,

with increasing massivity of the element it becomes more and more incorrect, thus leading to overestimation of the required reinforcement. In fact, the temperature variation in the cross-section, which is responsible for the formation of self-induced stresses, leads to the fact the tensile stresses develop only at some depth of the cross-section, while the interior of the wall is compressed (see Fig. 11). Localisation of the zero-stress (compensation) line is, however, extremally difficult to determine at the design stage as it would require to simulate the thermal field in the wall.

Another important aspect is the model from which the formula for the minimum required reinforcement was derived. The formula is based on the model of a tie, which does not represent the base-restrained elements well. That is because in the base-restrained elements the strains are confined not only by reinforcement, but also by the base, thus reducing the need for reinforcement. This fact is accounted for by CIRIA C766 where a reduction coefficient k_{Edge} has been introduced to represent this confining effect. The coefficient has been defined as $k_{\text{Edge}} = 1 - R_{\text{Edge}}$, where R_{Edge} is the degree of restraint at the base. With the increasing restraint the value of the coefficient – and consequently the required area of reinforcement – decrease.

5 Case study 2: heavily reinforced tank wall segment

5.1 Description of the structure

This case study was an internal segment of a wall in a rectangular reinforced concrete tank, restrained along the base and along both vertical edges, classified as semi-massive according to [34]. Cracking of the wall had been monitored for 9.5 months. Figure 9 schematically shows the geometry as well as cracking pattern and its change in time in the wall. In the first stage, the width of the cracks did not exceed 0.1 mm, they were mostly limited within a range of 0.025-0.05 mm, with individual cracks, not in numbers that could present a risk for compromising the integrity of the structure, of 0.075 mm width. At the second measurement stage, the measured crack widths only locally reached 0.15 mm, in other cases they were limited to 0.1 mm. At the last measurement stage, the crack widths did not increase. The data of the analysed case study including detailed description of the structure, its geometry, manufacturing technology as well as the measurements of development of hydration heat and mechanical properties, temperature development, shrinkage strains and creep under compression and

tension can be found in [41], [42], [43] and [44], while most important results are presented in the Appendix, sec. A.2.

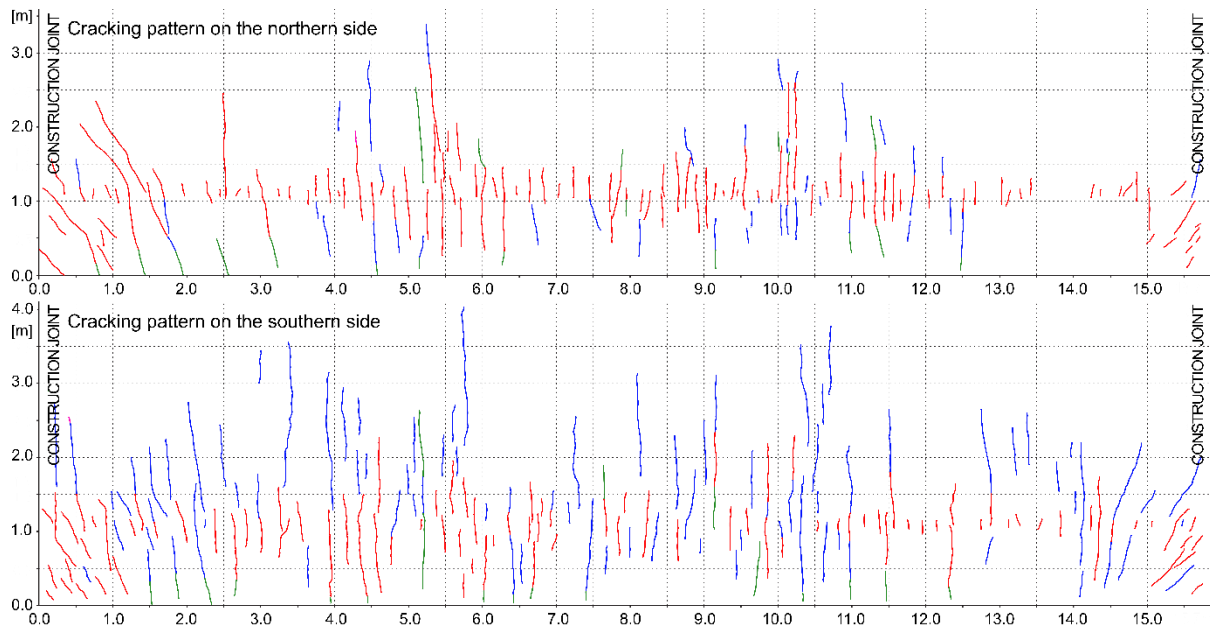
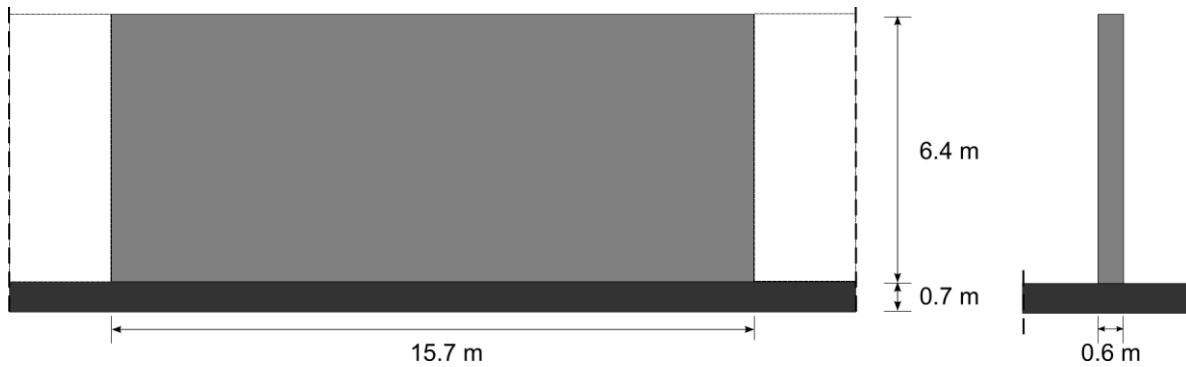


Figure 9. Tank wall segment: longitudinal view; cross-section; cracking pattern (16 days – red; 90 days – blue; 285 days – green).

5.2 Estimate of the early-age and long-term crack-inducing strain

The main purpose of the analysis of this case study is to compare the predictions of crack spacing and crack width change in time with developing strains using different methods. The calculations were therefore performed at two time instants: at the age of 16 days (early-age) and 90 days (long-term). It must be emphasised, however, that the first cracks appeared on the 2nd/4th day after casting while the measurements of the cracks width and spacing were only made after 16 days.

The strains were calculated at the height of +1.40 m above the joint, at the level where crack widths were measured. The temperature was taken as a mean temperature in the cross-section, determined from the measurements in points B3 (core) and B4 (northern surface) (see Fig. A.8) because of a relatively stable temperature distribution on that side of the wall. Drying shrinkage was also calculated as a mean value in the cross-section. Figure 10 shows the diagrams of the total shrinkage strain, thermal strain, autogenous shrinkage strain and drying shrinkage strain calculated in this point. Although at first glance difference can be observed between the measured and calculated total strain, it must be explained that the calculated thermal strain does not take into account the restraining effect, it is a theoretical strain in a completely unrestrained element. The measured total strain, in turn, includes the restraining effect, so the measured total strain represents only the unrestrained part of the sum of thermal and shrinkage strains. Given the roughly estimated value of the restraint factor (calculated with Eq. (2)) of 0.2 it can be demonstrated that the value of the restrained part of the total deformation is comparable to the calculated free shrinkage. Consequently, the value of the free shrinkage strain used in calculations were taken as 150 $\mu\epsilon$ at 16 days and as 395 $\mu\epsilon$ at 90 days.

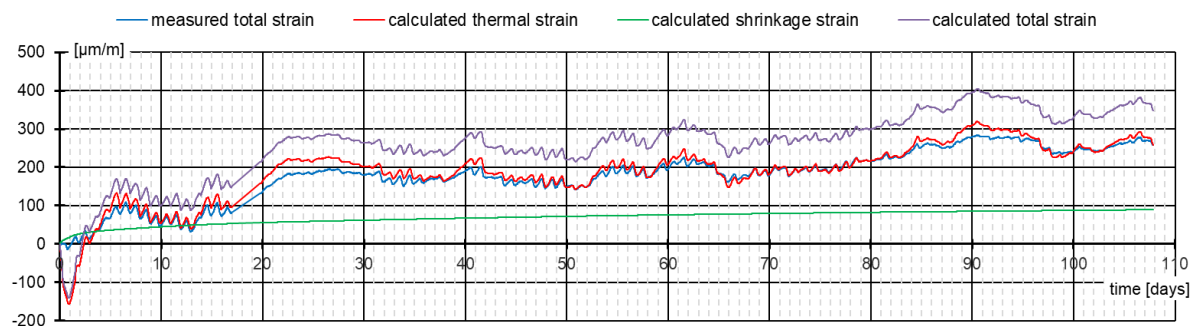


Figure 10. Calculated free imposed strain at the level of + 1.40 m in the tank wall segment.

It is very relevant at this point to discuss the issue of the degree of restraint which is one of the decisive factors in determination of the expected crack width (see Table 2). The width of the crack is expressed as dependent on the restrained part of strain with the use of the restraint factor R . The standards do not, however, differentiate the degree of restraint conditions before and after cracking – see e.g. recommendations of EN 1992-1-1:2023 [14] in Annex D where the same restraint factor is used both for the cracking risk assessment and the crack width.

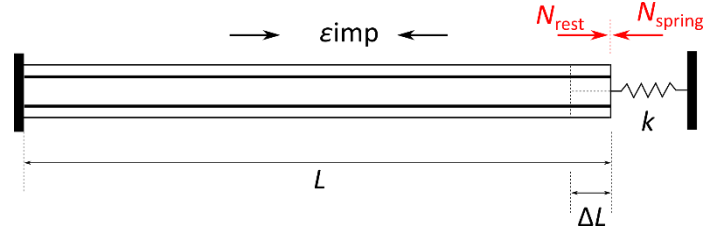


Figure 11. Equilibrium of forces and compatibility of deformations in a partially restrained tie under imposed shrinkage strain (after [45]).

The restraint factor is defined on the basis of strains by Eq. (2) which can be expressed on the basis of deformations as:

$$R = \frac{\varepsilon_{\text{imp}} \cdot L - \varepsilon_{\text{free}} \cdot L}{\varepsilon_{\text{imp}} \cdot L} = 1 - \frac{\Delta L}{\varepsilon_{\text{imp}} \cdot L} \quad (5)$$

where L is the length of the element and ΔL is its elongation due to imposed strain (see Fig. 1b). If the degree of external restraint is expressed with the stiffness of the spring k (Fig. 11), the conditions of equilibrium of forces $N_{\text{rest}} = N_{\text{spring}}$ and compatibility of deformations $\Delta L = \Delta L_{\text{spring}}$ can be defined.

With:

$$\Delta L = \varepsilon_{\text{imp}} \cdot L + \frac{N_{\text{rest}}}{E_c(t) A_c (1 + \alpha_e \rho)} \cdot L \quad (6a)$$

$$\Delta L_{\text{spring}} = \frac{N_{\text{spring}}}{k} \quad (6b)$$

the degree of restraint can be expressed as:

$$R = \frac{1}{1 + \frac{1}{k} \frac{E_c(t) \cdot A_c \cdot (1 + \alpha_e \rho)}{L}} \quad (7)$$

where $E_c(t) \cdot A_c \cdot (1 + \alpha_e \rho)/L$ is the axial stiffness of the element with respect to the included reinforcement. It can be noticed that in an uncracked element with the progressing time during hardening of concrete, due to the developing modulus of elasticity of concrete, the axial stiffness of the element will increase, thus the degree of restraint of the element decreases. However, once the cracking occurs, it will decrease the stiffness of the element, increasing the degree of restraint. This has been experimentally proven in [45].

When related to the actual case of a wall on foundation as the analysed case of a tank wall segment, the effect of increasing degree of restraint due to cracking can be illustrated with Fig. 12. Imposed deformations will cause tension over a certain height of the wall, and compression in the foundation,

which magnitude will increase with increasing imposed strains until tensile capacity of the wall is reached and a crack is formed. This will cause a relief of stresses immediately after cracking, both in the wall and in the foundation. This drop in the compressive stress in the foundation will lead to the extension of the foundation which, in turn, will cause additional opening of the crack, as a result of additional redistribution of imposed deformations. Therefore, if the width of the crack is to be calculated with the use of the approaches proposed in the standards, i.e. by applying the restraint factor for uncracked systems, then its magnitude in the cracked element must be higher than it would appear from the analysis of the uncracked element if the width of the crack is not to be underestimated.

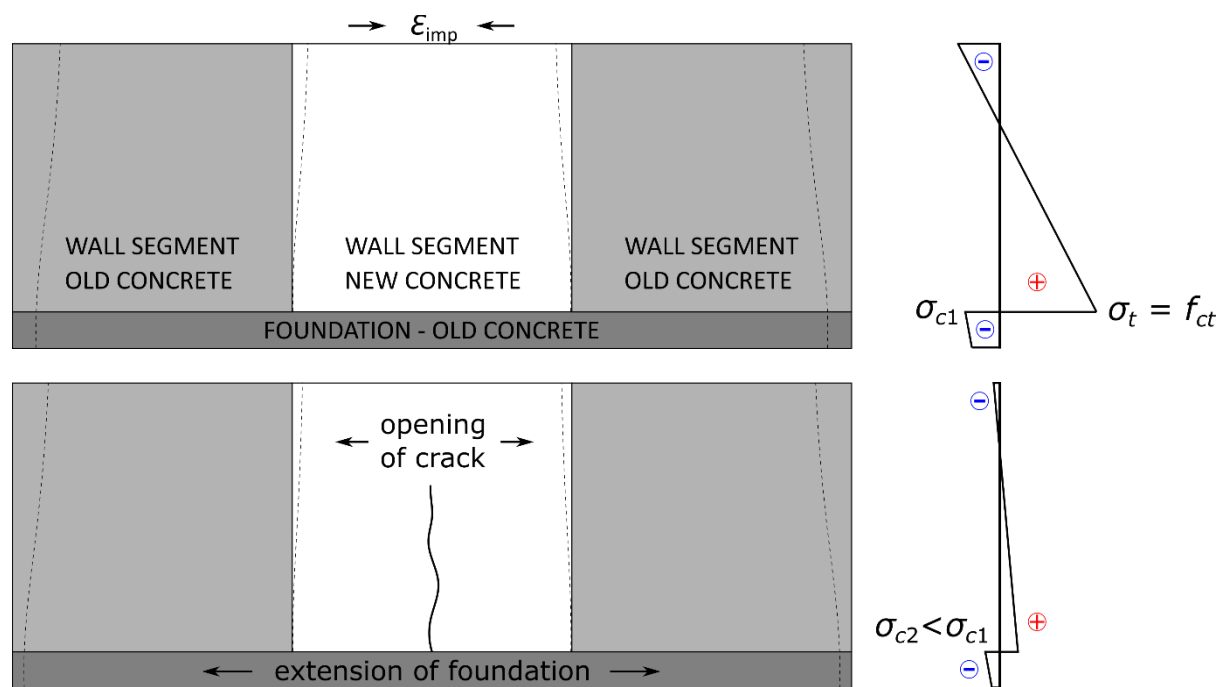


Figure 12. Changes of deformation and stresses in a wall subjected to imposed shrinkage strain: (top) right before cracking; (b) right after formation of a crack and stress relief.

Nevertheless, exact calculation of the value of the restraint factor in the cracked elements is a challenging task which requires further studies and authors are not yet confident to provide here a quantitative recommendation. Therefore, for now, a conservative value of the restraint factor in an uncracked state of 0.8 was used for further calculations at all stages of the crack width control.

The input data for calculation of the expected crack spacing and crack width as well as their change in time are collectively presented in Table 8.

Table 8. Input data for calculations of crack widths and their change in time in a tank wall.

	16 days	90 days
Source of load	Hardening temperature Autogenous shrinkage	Autogenous shrinkage Drying shrinkage Ambient temperature fluctuations
Imposed strain ε_{imp} [$\mu\varepsilon$]	150	395
Restraint factor R	0.8	0.8
Effect of creep K	0.65	0.60
Modulus of elasticity E_{cm} [GPa]	18.8	22.0
Tensile strength f_{ctm} [MPa]	1.61	1.99

The crack-inducing strain was calculated from the restrained part of strain and strain relief as recommended by the methods. The calculated strains are collectively presented in Table 9.

Table 9. Crack-inducing strain [$\mu\varepsilon$] in a tank wall segment calculated with different standardised methods.

Strains [$\mu\varepsilon$]	Restrained strain		Tensile capacity		Crack-inducing strain	
	16 days	90 days	16 days	90 days	16 days	90 days
EN 1992-1-1:2004 & EN 1992-3:2006	78*	190*	86	91	78	190
CIRIA C766	78*	190*	92*	127*	32	126
EN 1992-1-1:2023	78*	190*	86	91	27	135
CIA Z7/06	120	316	86	91	34	225
AIJ-SRC	n/a*	n/a*	100***	150***	351****	480****
ACI 207.2 & 224	120	316	100***	150***	20	166

* considers the effect of creep on reduction of strain;

** considers sustained character of loading and effective modulus of elasticity

*** recommended fixed value

**** crack formation stage assumption

Large differences between the expected values of the crack-inducing strain can be observed, even though the same values of the imposed strain and restraint factor were assumed in all the methods (for basic assumptions of the methods refer to Table 2). This is related to the way in which each method takes into account the effect of creep on the restrained strain and how it predicts the level of strain relief after cracking. In EN 1992-3:2006 the restraint factor is reduced to consider creep but no strain relief is taken into account, thus the value of the crack-inducing strain is the highest. In case of CIRIA C766 and EN 1992-1-1:2023, the level of extensibility is expected to be $0.5\varepsilon_{ctu}$ (46 and 63 $\mu\varepsilon$) and $0.6\varepsilon_{ctu}$

(51 and 54 $\mu\epsilon$), respectively, in addition to the same assumed reduction in the restraint factor, which explains lower values of crack-inducing strain. Finally, CIA Z7/06, AIJ-SRC and ACI 207.2 assume the level of extensibility at full ϵ_{ctu} . In case of CIA Z7/06 and ACI 207.2 no effect of creep is considered, so the methods predict by far the greatest values of the restrained strain but also the highest level of extensibility. As a results, the estimated values of the crack-inducing strain are in comparison moderate. Situation is different in case of the AIJ-SRC method which is based on the assumption of the crack formation phase. The crack-inducing strain, calculated considering creep, is much higher than predicted by other methods (even an order of magnitude at early age). However, its change in time is much less dramatic – the increase is by ~35% while for other methods the increase is from ~3 to even up to ~8 times.

5.3 Early-age and long-term crack width calculations

In the final step the crack spacing and crack width were calculated with the analysed methods with the focus on crack spacing and crack width change with the progressing increase of the imposed strains in time. The results of calculations are collected in Table 10.

Table 10. Early-age and long-term crack width in a tank wall segment.

	Crack spacing (mean) [cm]		Crack width (max) [mm]	
	16 days	90 days	16 days	90 days
measured	$s_{rm} = \sim 24$ cm	$s_{rm} = \sim 20$ cm	0.025–0.05, individual cracks 0.075	≤ 0.1 , individual cracks 0.15
EN 1992-1-1:2004 & EN 1992-3:2006	$s_{rm} = 17.6$ cm		0.023	0.057
CIRIA C766	$s_{rm} = 21.7$ cm		0.012	0.047
EN 1992-1-1:2023	$s_{rm} = 14.8$ cm		0.007	0.034
CIA Z7/06	$s_{rm} = 21.7$ cm		0.013	0.083
AIJ-SRC	$s_{rm} = 175.6$ cm	$s_{rm} = 36.7$ cm	0.057	0.078
ACI 207.2 & 224	$s_{rm} = 57.3$ cm	$s_{rm} = 11.3$ cm	0.019	0.032

It can be concluded that almost all the methods underestimated the crack widths to a probably problematic degree. Only the method of AIJ-SRC was somewhat closer to the measured value. With an accepted error of $\pm 20\%$ the predictions of this method would expect that majority of the cracks would

not exceed 0.057 mm and 0.078 mm, and would allow for the individual cracks of up to 0.068 mm after 16 days and 0.094 mm after 90 days, respectively.

The method of Eurocode 2 and all related to it, i.e. EN 1992-1-1:2004 & EN 1992-3:2006, CIRIA C766, EN 1992-1-1:2023 and CIA Z7/06, are based on the simplifying assumption of the same bond strength for the stabilised and the crack formation phase, and irrespectively of the level of imposed strain. This means that regardless of the crack stage the same formula is used for calculation of the crack spacing / transfer length ($s_{r,max} = 2l_{e,max}$). Hence, with the progressing imposed strain, the transfer length does not change and the width of the crack increases proportionally to the increase of the strain. Both EN 1992-1-1:2004 and EN 1992-1-1:2023 predict twice the transfer length to be lower than the measured crack spacing, especially EN 1992-1-1:2023, where the predicted spacing is 14.8 cm in relation to the measured values of 24 and 20 cm (Table 10), which may indicate that the wall had still been in the crack-formation stage. The low value of the transfer length might be one of the reasons for underestimation of the crack width, especially at early age.

In that sense the philosophy of the models implemented in AIJ-SRC and ACI 207.2 guidelines better reflects the actual behaviour of the wall where an increase in imposed strain caused not only widening of the existing cracks, but also formation of new cracks. Consequently, over the analysed period between 16th and 90th day the imposed strain increased over 2.5 times while the mean crack width only doubled which was associated with a decrease of mean crack spacing by almost 20%. This effect is observed in the predictions of both methods, however, in both cases the methods expect rather an increase in the number of cracks than an increase in their width. According to AIJ-SRC the increase in crack width is by 1.4 times while the decrease in spacing is by 5 times. In case of ACI 207 the increase in crack width is by 1.6 times with also the 5-time decrease in spacing. Nevertheless, due to ~3 times smaller crack spacings at both analysed time instants, the crack widths predicted by the ACI 207.2 method are ~3 times smaller than as per AIJ-SRC.

Another issue is that none of the crack models take into account larger shrinkage strains from drying that occur at the surface of the element. These models only take into account the mean value, which for the analysed wall may be several times smaller than the shrinkage at its surface. Thus, crack-inducing strain in the locations of crack width measurements are underestimated in these models. Additionally,

the precise determination of the restraint factor after cracking remains an open issue [46]. Currently, code models are based only on approximate values for an uncracked structure.

6 Conclusions and future work

The paper presents a critical analysis of the predictive capacity of standardised methods for crack width control in edge-restrained reinforced concrete elements subjected to imposed strains. The study covered relevant standardised methods implemented in the documents from Europe, Australia, Japan and the USA. The predicted crack widths were compared for the three distinct case studies: a theoretical demonstration example of a typical base-restrained wall, a massive wall on a raft foundation (Case study 1) and a heavily-reinforced semi-massive tank wall segment with combined restraint conditions (Case study 2). The study allowed to draw conclusions on the applicability of the methods for design of various externally restrained elements for serviceability limit state of cracking.

All the analysed models for determination of the crack spacing are based on the model of a tie. This can be a reasonable assumption to treat the element restrained along its edges as composed of the ‘slices’ behaving as ties, but only given that the actual degree of restraint is taken in calculations, not full fixation at its extremities. This is done only in the methods implemented in AIJ-SRC recommendation and ACI 207.2 report.

Furthermore, the cracking behaviour of the elements subjected to restrained imposed strains is governed by the crack formation stage. The increase in the restrained strain results both in the increase of the width of the existing cracks and formation of new cracks. The model for crack width control in such elements must, therefore, correspond to the expected cracking stage, which – among the analysed methods – is ensured only by the methods implemented in AIJ-SRC recommendation and ACI 207.2 report. The models proposed by EN 1992 standards family do not differentiate the length of the strains incompatibility section in the vicinity of the crack for different cracking stages, hence indicating that this length in the crack formation stage will be the same as in the stabilised cracking stage. It is known, however, that the bond strength depends on the cracking stage and consequently, the slip length is expected to be greater in the crack formation stage [47]. Therefore, the slip length calculated with the formula proposed by EN 1992 in case of the restraint-induced cracking may often lead to

underestimation of the crack width. This approach might be, however, useful for the design of restrained elements given that characteristics of these structures support the assumption of close-to-stabilised crack spacing. This includes the maintaining of a high degree of restraint during crack formation and/or high reinforcement ratio, as shown on the example of Case study 2. The expected final width of the crack may be then sufficiently well assessed.

Nevertheless, the typical cracking patterns of edge-restrained elements are not well represented by the assumption of the crack spacing in a stabilised crack pattern of a tie. As discussed in [48], the distance between primary cracks in a wall on foundation orientates predominantly on geometrical conditions of the element itself. Long walls are subject to through cracks over the entire wall with a crack distance of 1.2 times the wall height. Shorter walls, however, are rather subject to stopping cracks, whereby the crack distance is in the range of 1.2 times the crack height. For through cracks over the entire height of the wall the German Annex to EN 1992-1-1 [23] acknowledges this effect by proposing a crack distance of 2 times the wall height on the safe side. Nevertheless, using such a geometrically derived crack spacing in crack width calculations is only appropriate when applying deformation-compatible approaches with sufficient regard of the formation of secondary cracks in the vicinity of primary cracks, see e.g. [48].

Further, the transfer length is defined in relation to the ratio between the bar diameter and reinforcement ratio. Effective reinforcement ratio should be used which is related to the effective tensile area of concrete (actual zone of reinforcement impact). Some of the methods, e.g. AIJ-SRC, which are derived for relatively thin elements disregard the fact the effective tensile area becomes smaller than the concrete area with an increasing thickness of the wall, as shown on the example of Case study 1. Moreover, the height of the effective tensile area (depth of the reinforcement impact zone) is not a constant value dependent on the location of the reinforcement, but depends also on the thickness of the cross-section, which is encountered by the German Annex to EN 1992-1-1 [23].

Even though the philosophy of the model is crucial for the design, proper choice of the input parameters is of comparable importance. In both analysed case studies of real structures (Case 1 and 2) the calculated widths of the cracks were underestimated, which may have a number of reasons in addition to the underestimated crack spacing. First of all, the value of the imposed strain might be underestimated

by an assumption of a too low value of the coefficient of thermal expansion of concrete, which depends strongly on the type of the aggregate used. The value of the shrinkage strain, especially drying shrinkage strain, might be underestimated when mean value of shrinkage is taken in calculations while the magnitude of drying near the surface can be significantly higher.

Secondly, the value of the restraint factor can be wrongly estimated. A challenge might lay in proper assessment of the degree of restraint in non-standard restraining conditions, like the Case study 1 where the restraining body was of a relatively low stiffness but had a form of a common foundation slab. In semi-massive and massive walls which are most commonly subjected to imposed deformation, such as those analysed in Case study 1 and 2, there is also a combined effect of external restraint and internal restraint due to the strain variation in the cross-section. What is also not addressed by the analysed methods is the fact that the degree of restraint in a cracked element is different than in an uncracked element – it increases with the progressing cracking due to the reduction in stiffness of the element [45]. It is crucial to account for this fact in the design for crack control as the predicted width of the crack in all the analysed methods depends directly on the assumed degree of restraint.

Finally, the value of the calculated crack-inducing strain depends on the level of the assumed extensibility of concrete (ability of concrete to expand between the cracks) which is related to its tensile capacity. The recommended value of the strain relief may vary from 0 (EN 1992-1-1:2004) to $100\ \mu\epsilon$ at early age and $150\ \mu\epsilon$ in long term (ACI 207.2). The examples of Case study 1 show that when the design is performed based on the class of concrete, the extreme values of extensibility recommended by ACI 207.2 are overestimated. This observation is further enforced in the example of Case study 2 which shows that other mechanical properties (tensile strength, modulus of elasticity, tensile capacity) might be in reality lower than it would result from the predictions of the methods based on the compressive strength. This is a common case when admixtures are added to the concrete mix to obtain the required class. Therefore, a close cooperation between a designer and concrete technologist are required already at the design stage as the example of Case study 2 demonstrates that the design of special structures should not be based solely on the concrete class.

The above conclusions clearly show a need to develop a unified model for crack width control in edge-restrained reinforced concrete elements subjected to imposed strains. The model must take into account

the nature of cracking in edge-restrained elements (especially the influence of geometrical conditions on the distance between primary cracks and their growth over the wall), the actual stage of cracking and slip between the reinforcing bars and concrete (slip-dependent bond law). In addition, it should be generalised for various possible geometries and reinforcement, especially it should address the issues inherent to massive elements, heavily-reinforced elements and elements with combined restraint conditions. Furthermore, an agreement must be reached on the definition of the properties of concrete which should be taken for the design, including mechanical properties of concrete and creep. Finally, it is evident that a systematised study on the change of degree of restraint in walls during cracking is needed. In addition to the above, the effect of combination of the external loads and imposed deformations on prediction of the crack width is another complicated question that should be answered in the future.

Acknowledgements

The authors would like to acknowledge the support of: Dirk Schlicke (TU Graz, Austria), Andy Gardner (ARUP, Solihull, UK), Shingo Asamoto (Saitama University, Japan) and Tatsuya Usui (Taisei, Japan) in preparation of the paper, as well as the financial support of Arup.

Funding

This work was supported by the Polish Ministry of Education and Science through the Silesian University of Technology; FCT/MCTES through national funds (PIDDAC) under the R&D Unit Institute for Sustainability and Innovation in Structural Engineering (ISISE) [UIDB/04029/2020]; the Associate Laboratory Advanced Production and Intelligent Systems ARISE [LA/P/0112/2020].

CRedit author statement

Agnieszka Jędrzejewska: Conceptualization, Methodology, Formal Analysis, Investigation, Data curation, Writing – Original draft, Visualisation, Project administration **Mariusz Zych:** Conceptualization, Investigation, Resources, Writing – Review & Editing **Jean Michel Torrenti:** Resources, Writing – Review & Editing **Fragkoulis Kanavaris:** Conceptualization, Writing – Review & Editing, Funding acquisition **Miguel Azenha:** Conceptualization, Supervision, Writing – Review & Editing **Fangjie Chen:** Resources **Shintaro Ito:** Resources.

References

- [1] Jędrzejewska A, Kanavaris F, Zych M, Schlicke M, Azenha M. Experiences on early age thermal cracking of wall-on-slab concrete structures. *Struct* 27: 2520-2549 (2020); <https://doi.org/10.1016/j.istruc.2020.06.013>
- [2] Fairbairn EMR, Azenha M, eds. Thermal cracking of massive concrete structures. State-of-the-art Report of RILEM Technical Committee 254-CMS. Springer, Cham (2019); <https://doi.org/10.1007/978-3-319-76617-1>
- [3] Borosnyói A, Balazs GL. Models for flexural cracking in concrete: the state of the art. *Struct Concrete* 6(2): 53-62 (2005); <https://doi.org/10.1680/stco.2005.6.2.53>
- [4] Lapi M, Orlando M, Spinelli P. A review of literature and code formulations for cracking in R/C members. *Struct Concrete* 19: 1481-1503 (2018); <https://doi.org/10.1002/suco.201700248>
- [5] EN 1992-1-1:2004+A1:2014 – Eurocode 2. Design of concrete structures – Part 1-1: General rules and rules for buildings (2014).
- [6] EN 1992-3:2006 – Eurocode 2. Design of concrete structures – Part 3: Liquid retaining and containing structures (2006).
- [7] Bamforth PB. CIRIA C660: Early-age thermal crack control in concrete. CIRIA, London, UK (2007)
- [8] ACI 207.2R-07: Report on thermal and volume change effects on cracking of mass concrete (2007).
- [9] Guidelines for control of cracking of mass concrete 2016. Japan Concrete Institute, Technical Committee on English version of JCI guidelines for control of cracking of mass concrete (2017).
- [10] Klemczak B, Żmij A. Reliability of standard methods for evaluating the early-age cracking risk of thermal-shrinkage origin in concrete walls. *Constr Build Mater* 226: 651-661 (2019); <https://doi.org/10.1016/j.conbuildmat.2019.07.167>
- [11] Zych M. History of the development of analytical models of cracking of restrained walls on a given edge since 1968. *Int J Concr Struct M* 16 (2022); <https://doi.org/10.1186/s40069-022-00555-3>

- [12] Jędrzejewska A, Zych M, Kanavaris F, Chen F, Ito S, Torrenti J-M, Schlicke D, Asamoto S, Azenha M. Standardised models for cracking due to restraint of imposed strains – the state of the art. *Struct Concrete* 24(4): 5388-5405 (2023); <https://doi.org/10.1002/suco.202200301>
- [13] FprEN 1992-1-1:2022 [Final draft] – Eurocode 2: Design of concrete structures – Part 1-1: General rules – Rules for buildings, bridges and civil engineering structures (Nov 2022)
- [14] EN 1992-1-1:2023 – Eurocode 2: Design of concrete structures – Part 1-1: General rules – Rules for buildings, bridges and civil engineering structures (Nov 2023).
- [15] Bamforth P. CIRIA C766: Control of cracking caused by restrained deformation in concrete. CIRIA, London, UK (2018)
- [16] CIA Z7/06 – Concrete cracking and crack control, Concrete Institute of Australia (2017)
- [17] Architectural Institute of Japan: Recommendations for practice of crack control in reinforced concrete buildings (Design and construction), 2006. [in Japanese]
- [18] ACI 224R-01: Control of cracking in concrete structures (2001, Reapproved 2008)
- [19] ACI 207.2R-95: Effect of restraint, volume change and reinforcement on cracking of mass concrete (1995; Reapproved 2005)
- [20] El Khoury K, Ridley I, Vollum R, Forth J, Shehzad M, Elwakeel A, Nikitas N, Izzuddin B. Experimental assessment of crack width estimations in international design codes for edge restrained walls. *Structures* 55: 1447-1459 (2023); <https://doi.org/10.1016/j.istruc.2023.06.087>
- [21] Klausen A. Early age crack assessment: codes, guidelines and calculation methods. DaCS Report np. 02. SINTEF Building and Infrastructure, Trondheim, Norway (2018). Available online: <https://www.sintef.no/contentassets/a2c5a98a03594086b7e6e872c02f39f7/dacs-report-no-2-wp1.2-early-age-crack-assessment.pdf>, last accessed on 18/08/2023
- [22] CROW-CUR Report 1:2020 – Crack width control of concrete structures (2020) [unpublished]
- [23] DIN EN 1992-1-1/NA:2013-04: National Annex to EN 1992-1-1: Design of concrete structures – Part 1-1: General rules and rules for buildings (2013)
- [24] Carino NJ, Clifton JR. Prediction of cracking in reinforced concrete structures. NISTIR 5634. Building and Fire Research Laboratory, National Institute of Standards and Technology,

923 Gaithersburg, (1995). Available online:
 924 <https://nvlpubs.nist.gov/nistpubs/Legacy/IR/nistir5634.pdf>, last accessed on 18/08/2023.

925 [25] Gilbert RI. Shrinkage cracking in fully restrained concrete members. ACI Struct J 89(2): 141–149
 926 (1992); <https://doi.org/10.14359/2917>

927 [26] Base GD, Murray MH. Controlling shrinkage cracking in restrained reinforced concrete.
 928 Proceedings of the 9th Australian Road Research Board (ARRB) Conference. Volume 9. Brisbane,
 929 Australia: ARRB, p. 167–73 (1978)

930 [27] Schlicke D, Dorfmann EM, Fehling E, Tue NV. Calculation of maximum crack width for practical
 931 design of reinforced concrete. Civil Engineering Design 3: 45–61 (2021)
 932 <https://doi.org/10.1002/cend.202100004>

933 [28] Tan R, Hendriks M, Geiker M, Kanstad T. Analytical calculation model for predicting cracking
 934 behavior of reinforced concrete ties. Journal of Structural Engineering (United States) 146(2):
 935 04019206 (2020) [https://doi.org/10.1061/\(ASCE\)ST.1943-541X.0002510](https://doi.org/10.1061/(ASCE)ST.1943-541X.0002510)

936 [29] Somma G, Vit M, Frappa G, Pauletta M, Pitacco I, Russo G. A new cracking model for concrete
 937 ties reinforced with bars having different diameters and bond laws. Engineering Structures 235:
 938 112026 (2021) <https://doi.org/10.1016/j.engstruct.2021.112026>

939 [30] EN 206:2013+A2:2021 – Concrete – Specification, performance, production and conformity
 940 (2021)

941 [31] ACI 209.2R-08: Guide for modeling and calculating shrinkage and creep in hardened concrete
 942 (2008)

943 [32] Azenha M, Kanavaris F, Schlicke D, Jędrzejewska A, Benboudjema F, Honorio T, Šmilauer V,
 944 Serra C, Forth J, Riding K, Khadka B, Sousa C, Briffaut M, Lacarrière L, Koenders E, Kanstad T,
 945 Klausen A, Torrenti J-M, Fairbairn EMR. Recommendations of RILEM TC 287-CCS: thermo-
 946 chemo-mechanical modelling of massive concrete structures towards cracking risk assessment.
 947 Mat Struct 54: 135 (2021); <https://doi.org/10.1617/s11527-021-01732-8>

948 [33] Knoppik-Wróbel A, Klemczak B. Degree of restraint concept in analysis of early-age stresses in
 949 concrete walls. Eng Struct 102: 369-386 (2015); <https://doi.org/10.1016/j.engstruct.2015.08.025>

- [34] Kanavaris F, Jędrzejewska A, Sfikas IP, Schlicke D, Kuperman S, Šmilauer V, Honório T, Fairbairn EMR, Valentim G, Funchal de Faria E, Azenha M. Enhanced massivity index based on evidence from case studies: Towards a robust predesign assessment of early-age thermal cracking risk and practical recommendations. *Const Build Mater* 271: 121570 (2021); <https://doi.org/10.1016/j.conbuildmat.2020.121570>
- [35] *fib* Bulletin 13: Nuclear containments (2001)
- [36] Benboudjema F, Torrenti JM. Early-age behavior of concrete nuclear containments. *Nucl Eng Des* 238(10):2495-2506 (2008); <https://doi.org/10.1016/j.nucengdes.2008.04.009>
- [37] Granger L. Comportement différé du béton dans les enceintes de centrales nucléaires: analyse et modélisation. PhD Thesis, Ecole Nationale des Ponts et Chaussées, France (1995) [in French]
- [38] Ithurrealde G, de Larrard F, Nectoux J: Bétons à hautes performances (BHP) pour l'étanchéité des structures en béton. Expérimentation. *Annales de l'Institut technique du bâtiment et des travaux publics* 502:77-115 (1992)
- [39] Buffo-Lacarriere L, Sellier A, Turatsinze A, Escadeillas G. Finite element modelling of hardening concrete: application to the prediction of early age cracking for massive reinforced structures. *Mater Struct* 44:1821-1835 (2011); <https://doi.org/10.1617/s11527-011-9740-y>
- [40] Beeby AW. Fixing in cracked concrete – The probability of coincident occurrence and likely crack width. CIRIA, London, UK (1990)
- [41] Seruga A, Zych M. Research on thermal cracking of a rectangular RC tank wall under construction. I: Case study. *J Perform Constr Fac* 30(1): 04014198 (2016); [https://doi.org/10.1061/\(ASCE\)CF.1943-5509.0000704](https://doi.org/10.1061/(ASCE)CF.1943-5509.0000704)
- [42] Zych M. Case study of concrete mechanical properties development based on heat temperature measurements. *Cement Lime Concrete* 20(6): 383-392 (2015).
- [43] Zych M, Seruga A. A new model for crack control in reinforced concrete tank walls. Part II: Comparison with experimental results. *ACI Struct J* 116(3): 95-105 (2019); <https://doi.org/10.14359/51713317>
- [44] Seruga A, Zych M. Research of concrete creep at early age under compressive and tensile stresses. *Cement Lime Concrete* 21(2): 65-77 (2016).

- 978 [45] Schlicke D, Hofer K, Tue NV. Adjustable restraining frames for systematic investigation of
979 cracking risk and crack formation in reinforced concrete under restrained conditions. In: M. Serdar
980 et al. (eds.), Advanced Techniques for Testing of Cement-Based Materials, Springer Tracts in Civil
981 Engineering. Springer, Cham, pp. 211-239 (2020); https://doi.org/10.1007/978-3-030-39738-8_7
- 982 [46] Zych M. The effect of the degree of cracking on the state of stress and cracks width in elements
983 with restrained boundary conditions. Structural Concrete 24(6): 7091–7102 (2023);
984 <https://doi.org/10.1002/suco.202300362>
- 985 [47] *fib* Model Code 2010, 2013
- 986 [48] Schlicke D. Mindestbewehrung zwangbeanspruchter Betonbauteile unter Berücksichtigung der
987 erhärtungsbedingten Spannungsgeschichte und der Bauteilgeometrie. PhD Thesis, Graz University
988 of Technology, Graz, Austria (2014) [in German]

APPENDIX: Detailed descriptions of Case studies

A.1 Case study 1: Massive wall of Civaux NPP mock-up

The analysed wall was an experimental mock-up nuclear containment wall tested by EDF in early 1980s within the THM (thermo–hydro–mechanical) task of the CEOS.fr project related to safety analysis of a newly constructed nuclear power plant near Civaux, France. The wall was 1.2 m thick, 2.8 m high (in total, divided into two lifts of 1.9 m and 0.9 m) and 20 m long, supported on a 0.4 m-thick raft foundation (see Fig. A.1). Breaks between the execution of the following segments were ~2 weeks. The main reinforcement of the wall was $\varnothing 20$ bars spaced vertically by 200 mm and horizontally by 180 cm (steel strength $f_{yk} = 400\text{MPa}$ and modulus of elasticity $E_s = 203\text{ GPa}$ with 5 cm concrete cover – see Fig. A.2). Vertical tubes for prestressing were also installed at the depth of 50 cm, spaced at ~80 cm. The wall was made with OPC concrete whose details of mix composition and resulting properties are enlisted in Table A.1.



Figure A.1. Geometry of the Civaux mock-up wall: (a) longitudinal view; (b) cross-section.

Table A.1. Composition and mechanical properties of concrete used for a Civaux mock-up wall [35].

Composition [kg/m ³]		Characteristics and results	
Aggregate	1872	Density [t/m ³]	2.33
Filler (limestone)	0	28-day compressive strength [MPa]	40.2
Silica fume	0	28-day tensile strength [MPa]	3.7
Cement CEM II/A 42.5R	350	28-day modulus of elasticity [GPa]	33.7
Water	195	Coefficient of thermal dilation [1/°C]	10×10 ⁻⁶
Superplasticiser	1		

The wall was equipped with thermocouples to follow the evolution of the temperature in different locations – Figure A.3 shows the locations of thermocouples while Figure A.4 shows the diagrams of temperature development in chosen points in the wall (valid measurements only). The initial

temperature of concrete of the wall was 19°C while the temperature of the foundation, which had already been hardened and pre-cooled to the temperature of the environment at the moment when the wall was cast, was 7°C. The formwork was removed after 5 days and at that moment the measurements stopped. The wall heated up to the maximum of almost 60°C and the difference between the core and near-surface temperature was ~6°C.

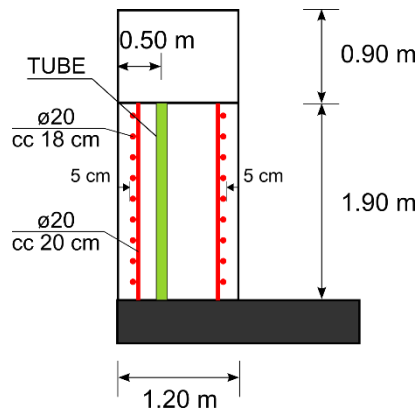


Figure A.2. Details of reinforcement in the Civaux mock-up wall (lift 1 only).

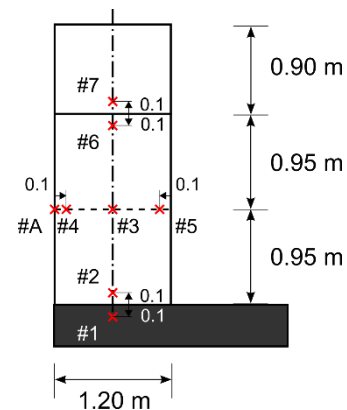


Figure A.3. Locations of thermocouples in the Civaux mock-up wall.

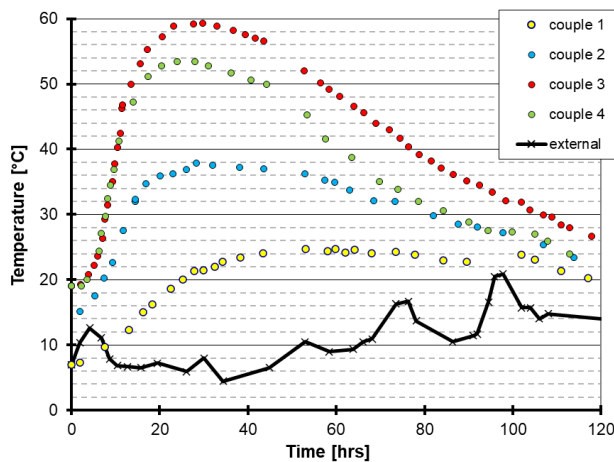


Figure A.4. Temperature development in the Civaux mock-up wall [36].

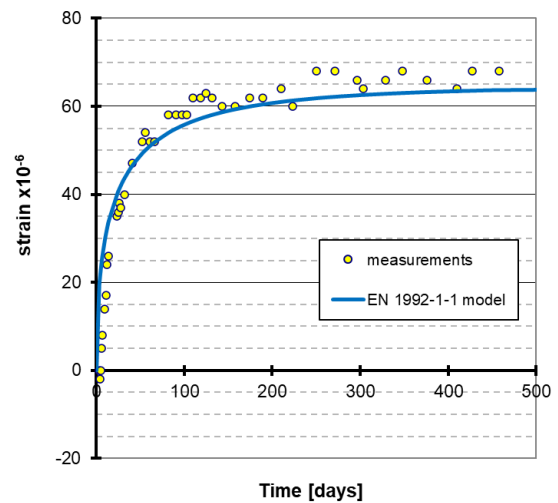


Figure A.5. Autogenous shrinkage strains of concrete used in the Civaux mock-up wall [37].

The measurement of autogenous shrinkage was performed independently in the laboratory on the exact same concrete mix as used for the construction of the wall. The tests were carried out on the cylindrical samples of $\phi 16$ cm diameter and 1 m length, and the measurements were made in the central part of the

sample. Figure A.5 presents the results of the measurement of autogenous shrinkage strains. The measurements were approximated with the function proposed by EN 1992-1-1:2004 [5] as:

$$\varepsilon_{ca}(t) = [1 - \exp(-0.2 \cdot t^{0.5})] \cdot \varepsilon_{ca,\infty} \quad (\text{A.1})$$

where the final value of the autogenous shrinkage was determined to be $\varepsilon_{ca,\infty} = 64.6 \mu\epsilon$.

Drying shrinkage was not taken into account because cracking was formed before drying began (before removing the formwork).

Figure A.6 shows the cracking pattern in a Civaux mock-up wall. 8 cracks were formed which location at both surfaces of the wall indicated that the cracks were through. The cracks were in general spaced by 1.6 / 2.4 / 3.2 m, which corresponds to 2×, 3× and 4× the spacing of the vertical tubes for prestressing. The widths of the cracks were $1 \times 0.04 \text{ mm}$, $4 \times 0.1 \text{ mm}$, $2 \times 0.2 \text{ mm}$ and $1 \times 0.5 \text{ mm}$. Unfortunately, it has not been specified what was the exact width of particular cracks and which crack had an excessive width of 0.5 mm.

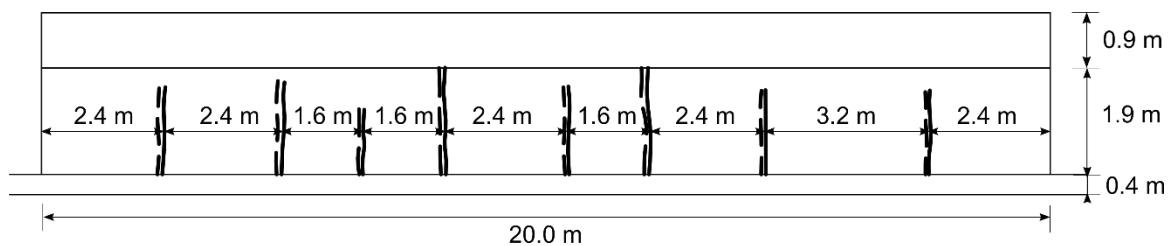


Figure A.6. Cracking pattern in the Civaux mock-up wall [36][38].

The *a posteriori* numerical analyses of the wall [36] [39] confirmed the observed cracking pattern and that the cracks were through cracks. According to the results of these simulations, due to the fact that the wall was kept in the formwork over the cooling phase, higher tensile stresses developed in the interior of the wall where crack formation initiated in the core of the wall, additionally aided by weakening of the cross-section by the location of the vertical tubes (“grooves”). Soon after, cracking penetrated towards the surfaces of the wall. Even though the effect of external restraint could be regarded as weak because of a relatively low thickness of the foundation with respect to the wall, it must be remembered that the wall was cast on a common raft plate. As a consequence, the external restraint was responsible for the fact that the formed cracks reached the joint while the length-to-height ratio > 10 led to the cracks developing significant heights ($> 80\%$ height of the wall) with some cracks over the whole height of the lift.

A.2 Case study 2: heavily reinforced tank wall segment

This case study is an internal segment of a semi-massive wall in a rectangular reinforced concrete tank, restrained along the base by a foundation slab and along both vertical edges by previously executed wall segments. Cracking of the wall had been monitored for 9.5 months. During this period, both early-age and long-time strains occurred, which were related to concrete shrinkage and changes in ambient temperature in the winter.

The discussed tank with horizontal dimensions of 96.90×50.40 m and a wall height of 6.9 m was executed without expansion joints. The length of the analysed segment was 15.7 m and its height without slants and the crowning beam was 6.4 m (Fig. A.7). The wall had a thickness of 60 cm.

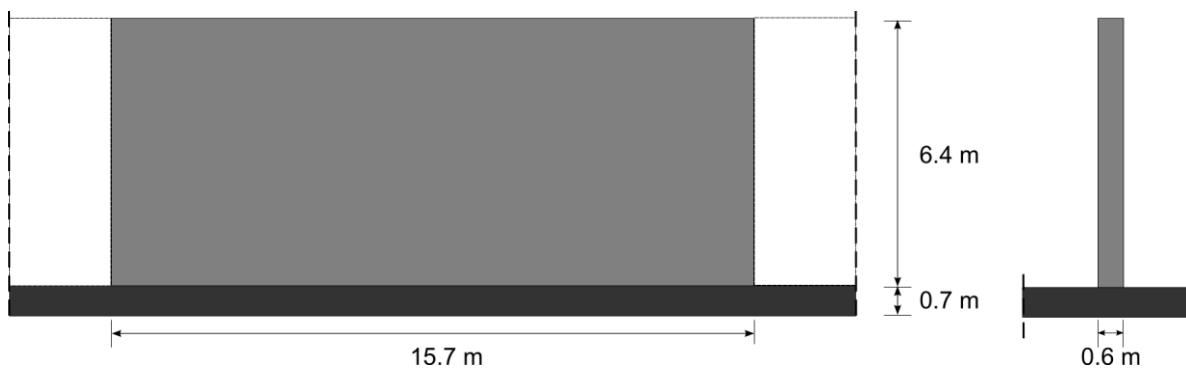


Figure A.7. Geometry of the tank wall segment: (a) longitudinal view; (b) cross-section.

The composition of the concrete mix for the execution of C30/37 class concrete is shown in Table A.2. Tests results of compressive strength, tensile strength and modulus of elasticity of concrete are summarised in Table A.3. It should be emphasised that the concrete mix was designed to satisfy the requirements of the class, hence the 28-day compressive strength reached 32 MPa, but the value of the mean modulus of elasticity and mean tensile strength measured for this concrete were lower than one would predict with e.g. EN 1992-1-1:2004.

Table A.2. Composition of concrete mix used in construction of the tank [41].

Concrete mix component	Content [kg/m ³]
Cement CEM III/A 32.5N (36-65% GGBFS)	380
Gravel 8/16	641
Gravel 2/8	439
Sand 0/2	619

Water	175
FM 21	4.56
LP 70	0.87
Air content [%]	4.5

Table A.3. Mechanical properties of concrete used in construction of the tank [41].

Concrete age [days]	1	1.5	2	3	4	5	7	14	28	60	90
f_{ck} [MPa]	3.3	---	6.13	8.18	9.73	11.54	15.32	23.7	32	---	---
E_{cm} [GPa]	6.9	---	11.25	12.25	13.6	14.7	16.55	18.65	20.55	---	22
f_{ctm} [MPa]	---	0.74	0.92	---	1.1	1.26	1.44	---	1.71	1.84	1.99

In order to be able to determine the values of the mechanical properties at various time instants, the results of measurements were represented with the time development function:

$$f_i(t) = \left[\exp \left[s_i \cdot \left(1 - \sqrt{\frac{28}{t}} \right) \right] \right]^{n_i} \cdot f_i(28) \quad (\text{A.2})$$

where f_i is the mechanical property of concrete: tensile strength, modulus of elasticity and tensile capacity, respectively. This formula was adopted from EN 1992-1-1. In Eq. (A.2) $f_i(28)$ is the value of the given property at the age of 28 days, while coefficients s_i and n_i allow to calibrate the rate of development of each property. The values of relevant parameters in Eq. (A.2) determined using the least square approximation are collectively presented in Table A.4.

Table A.4. Parameters of the time-development function of mechanical properties of the tank wall concrete.

Modulus of elasticity			Tensile strength		
$E_c(28)$ [GPa]	s_E	n_E	$f_t(28)$ [MPa]	s_f	n_f
20.65	0.67	0.36	1.74	0.61	0.40

The layout of the reinforcement in the wall is illustrated in Fig. A.8. The steel of A-III/RB400W class was used ($f_{yk} = 350$ MPa). Up to the height of 2.0 m the wall was reinforced in two layers, i.e. $\varnothing 20$ every 100 mm and $\varnothing 20$ every 150 mm ($\rho = 1.74\%$). Above 2.0 m, the reinforcement was placed in one layer, i.e. $\varnothing 20$ every 100 mm ($\rho = 1.05\%$). Concrete cover was 40 mm.

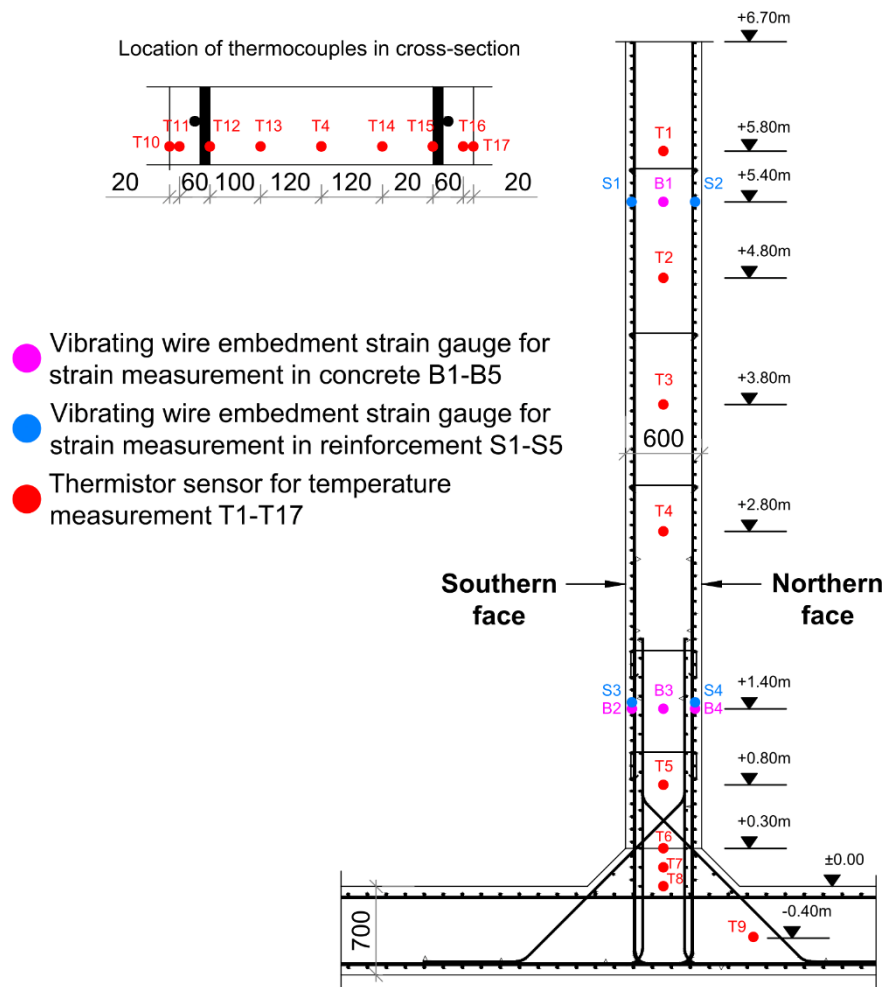


Figure A.8. Reinforcement layout and arrangement of measuring sensors in the tank wall segment.

The analysed segment was concreted in summer. The formwork on the southern wall surface was removed after 20 hours while on the northern surface after 40 hours. Measurements of strains with Demec strain gauge were carried out after the formwork had been removed from the wall along its entire length at a height of 1.1 m above the upper surface of the slant (level + 1.40 m).

Figure A.9 illustrates the cracking pattern and its development from 16 days, through 90 days up to 285 days. First cracks appeared 2 days and 4 days after casting of the tank wall segment on the southern and northern side, respectively. It was characteristic that the first cracks occurred in large numbers, but their lengths and widths were very limited (0.025 to 0.075 mm). The reason behind this was partly the high ratio of wall reinforcement ($\rho = 1.74\%$) and a significant contribution of self-equilibrating stresses. The difference in the crack formation process on the northern and southern surfaces resulted from different time of removing the formwork from both surfaces. It was found that in this first stage of measurements (i.e. after 16 days), the widths of the cracks did not exceed 0.1 mm.

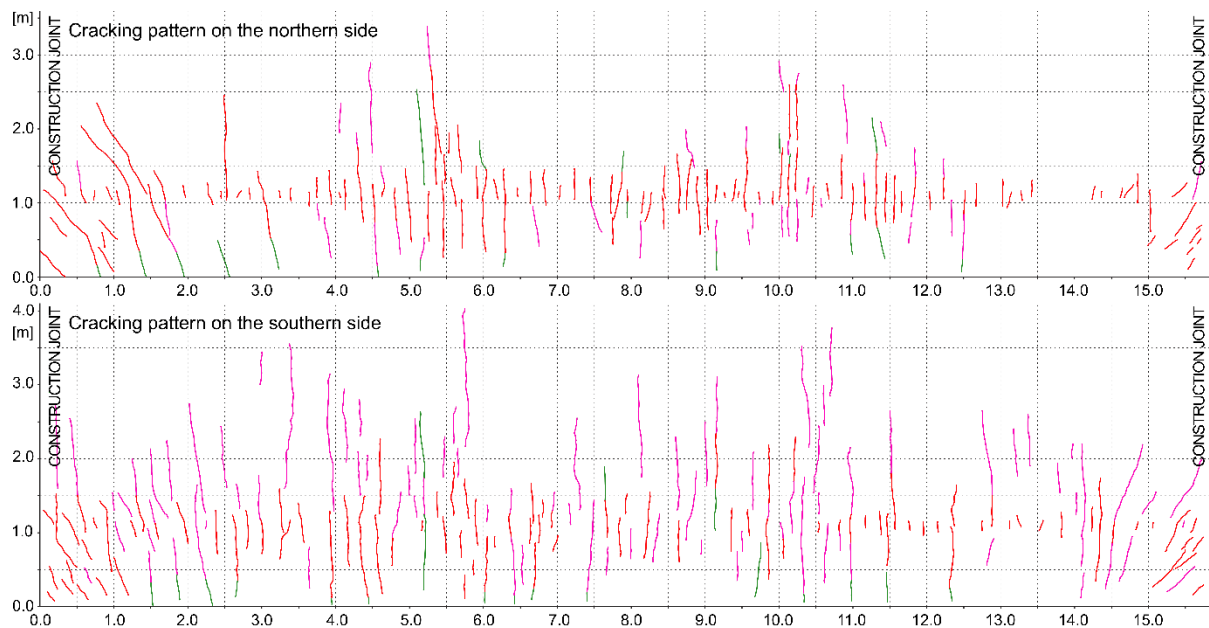


Figure A.9. Stages of cracking of the tank wall segment: a) northern surface, b) southern surface. (16 days – red; 90 days – pink; 285 days – green).

Comparing the change in the crack layout in the period from the 16th day after concreting to the crack layout after 3 months (see Fig. A.9), i.e. the period in which only additional imposed strains occurred, a significant increase in the number of cracks and their length up to 4.0 m on both surfaces was noticeable. During this period, the average crack spacing was reduced from 0.24 m to 0.20 m, the crack widths locally reached 0.15 mm, and in other cases they would be limited to 0.1 mm.

The final stage of crack formation was surveyed after 9.5 months. This stage included the water-tightness test of the tank and further imposed strains. Comparing this period with the period of 3 months, a small number of new cracks and the elongation of a few cracks towards the lower edge of the wall were observed. In this last stage of the measurements the crack widths did not increase. 9.5 months after concreting the wall at the level of 1.1 m the measured mean crack spacing was 0.174 m on the northern surface of the wall and 0.187 m on the southern surface. Only on the southern surface, the average crack width was locally exceeding 0.1 mm.

The temperature was measured in several points on the wall located both along its height and its thickness (see Fig. A.8). The measured temperature changes and distribution in the period of concrete hardening and over the period of 4 months are presented in Fig. A.10 and Fig. A.11.

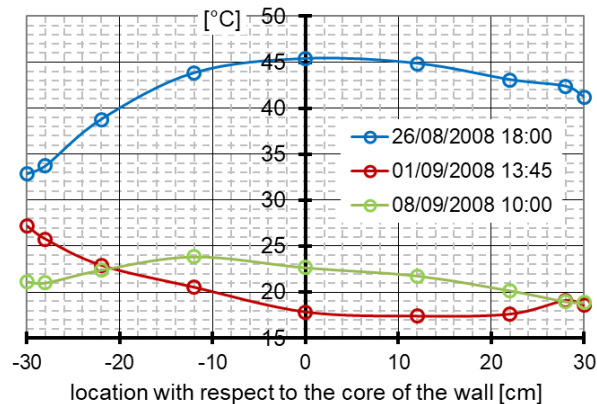
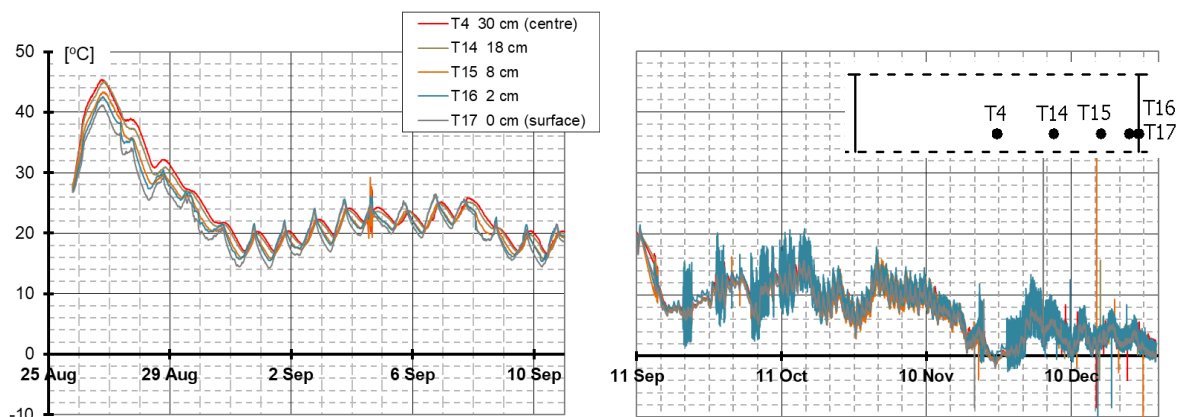
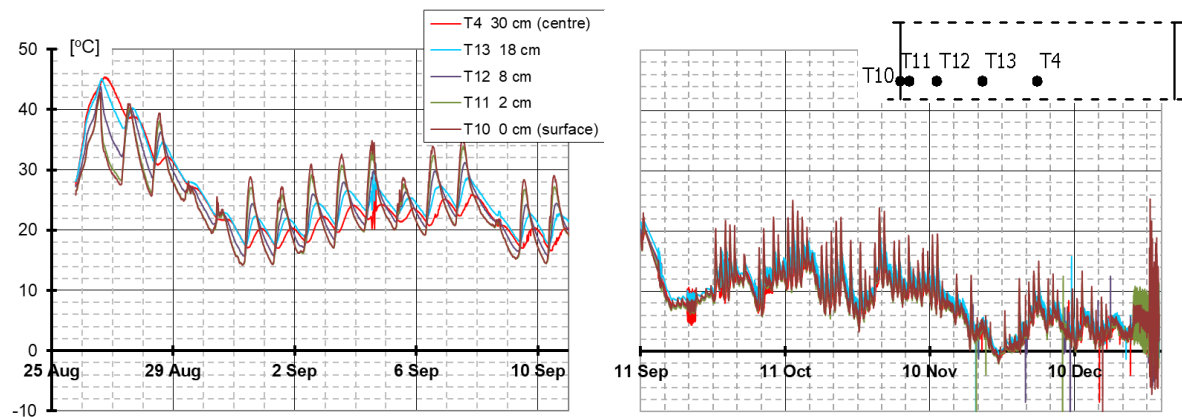


Figure A.10. Temperature measured at the thickness of the wall and its change in time

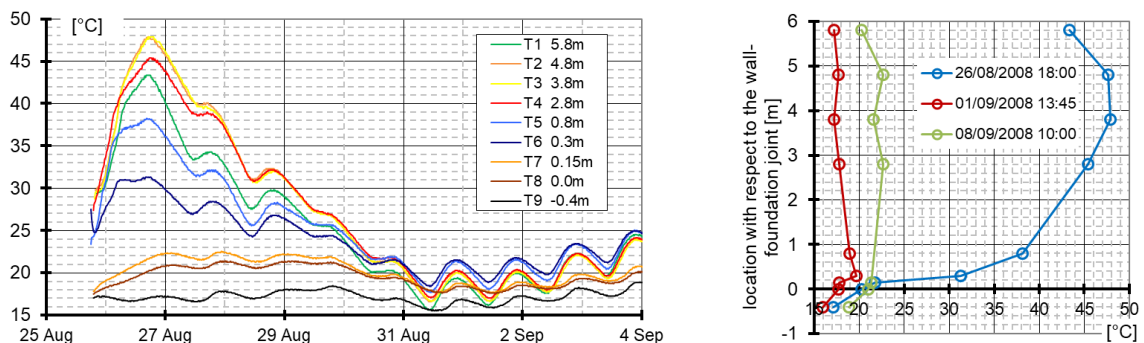


Figure A.11. Temperature measured along the height of the wall and its change in time

The maximum hardening temperature of $\sim 48^{\circ}\text{C}$ was reached after approximately 24 hrs in the core of the wall (Fig. A.10). It is interesting to notice that the temperature at that moment was the highest at a relatively high level ($\sim 0.7H$) above the joint (Fig. A.11). Regarding the temperature difference in the cross-section, an important influence of diurnal temperature fluctuations and exposure was visible (Fig. A.10). Because of a relatively small thickness of the wall, at the time of the maximum temperature occurrence (Aug 26), the temperature difference between the core and the surface was at the level of up to $\sim 6^{\circ}\text{C}$ on the northern side of the wall, while on the southern, exposed side these differences reached even up to $\sim 15^{\circ}\text{C}$.

After about 6 days the wall cooled down and its temperature was affected only by the ambient temperature, which oscillated around 20°C over the next 10 days (Fig. A.10). The temperature along the height of the wall in its core was almost uniform (Fig. A.11). In the long-term analysis of the temperature change it can be noticed that the wall was affected not only by the strains caused by the temperature drop but also temperature gradients in the cross-section. The differences between the core and surface temperature on the northern side did not exceed 3°C while on the southern side of the wall reached periodically even up to several degrees. It is interesting to notice the effect of exposure of the southern side – during the day the surface of the wall on this side was intensively heated by the sun which caused higher temperatures on the surface than in the core (Fig. A.10). Similar effect can be seen on the northern surface, but it is of much smaller magnitude. Over the period of the analysis the temperature of the wall decreased to almost 0°C (Fig. A.10), which means the temperature drop of almost 50°C .

Laboratory shrinkage strain measurements were performed on the concrete used for construction of the analysed tank wall segment. The tests were performed on the $10\text{ cm} \times 10\text{ cm}$ beams. Figure A.12 presents the results of the measurements of the total strain for 8 months.

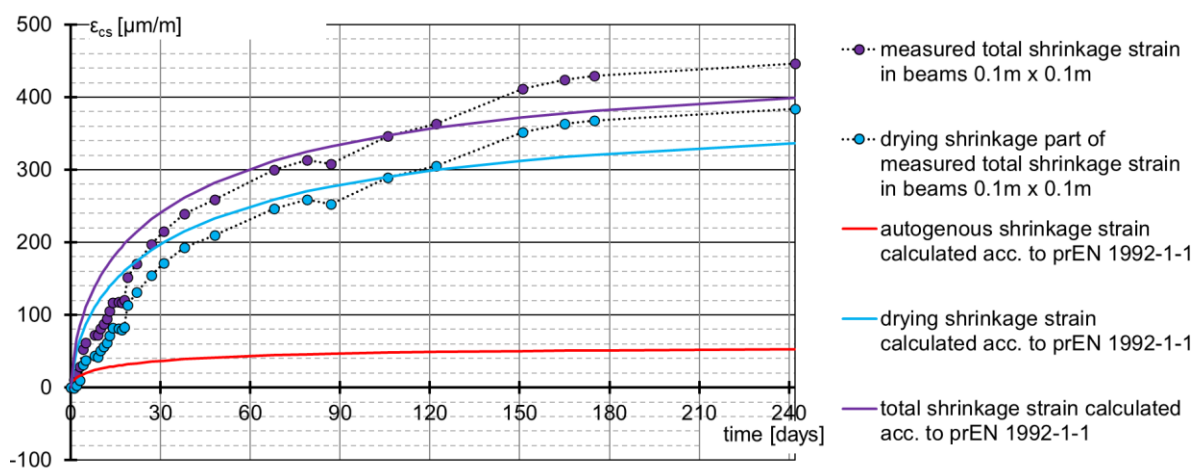


Figure A.12. Shrinkage strain of concrete used for construction of the tank wall measured in the laboratory conditions and approximated with EN 1992-1-1:2023.

Concrete strain measurements were also carried out on the wall with the use of embedment vibrating wire sensors (for the arrangement see Fig. A.8). The first group of sensors was placed at the height of +1.40 m. The second group of sensors was located in the upper part of the wall 1.3 m below the lower edge of the crowning beam (at the level of + 5.40 m), which is the zone that usually does not crack, thus allows to perform linear analysis. Figure A.13 presents the measurements of strains over the period of first 4 months. This strain can be understood as a free part of the restrained strain. Therefore, it can be observed that the biggest values of strains were recorded in the top part of the wall (at the level of +5.40 m) while the strains near the joint (at the level of + 1.40 m), where the level of restraint was lower, were smaller. This was also the zone of the wall which cracked.

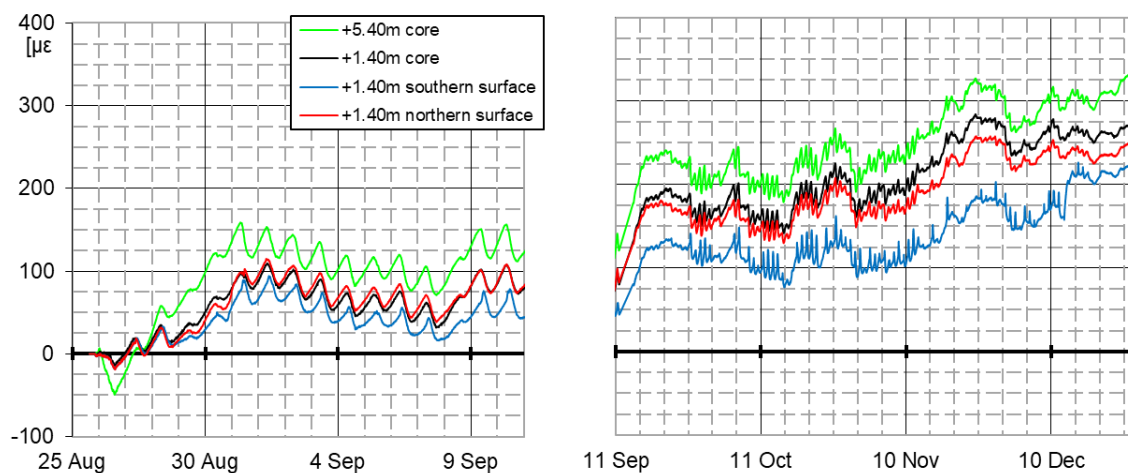


Figure A.13. Changes of measured strains in concrete over 4 months.

The measured concrete strains were compared with the calculated strains. The total free strain was calculated as a sum of thermal strain, determined from the temperature change, and shrinkage strain, calculated based on the laboratory tests results. Calculations were performed in point where the B1 sensor was located to compare the results with the measured strains. The thermal strain was calculated by multiplication of the temperature difference measured in the point B1, calculated in time steps of 15 mins, by the coefficient of thermal expansion which value was taken as $10^{-5}/^{\circ}\text{C}$. Measurements of strains were sparser than the measurements of temperature. Therefore, it was necessary to define an approximation function to obtain intermediate results. The formulas proposed by EN 1992-1-1:2023 were used as they offer an improved prediction of shrinkage strains in comparison to EN 1992-1-1:2004. The approximation functions used in calculations are shown in Fig. A.12.

The autogenous shrinkage development was approximated with a function:

$$\beta_{ca}(t) = 1 - \exp(-0.2\sqrt{t}) \quad (\text{A.3})$$

and the final value of the autogenous shrinkage determined for the applied class of concrete was $65 \mu\epsilon$. The autogenous shrinkage in the wall was calculated considering temperature dependence of the development rate using an equivalent age of concrete instead of the time based on the recorded temperature history. Autogenous shrinkage calculated with this approach was subtracted from the total measured shrinkage, and the result was treated as drying shrinkage part of the strain.

The drying shrinkage development was approximated with the function:

$$\beta_{cd}(t) = \left[(t - t_s) / (t - t_s + 0.035h_0^2) \right]^{0.5} \quad (\text{A.4})$$

with the final value of drying shrinkage equal to $393 \mu\epsilon$ and coefficient $\beta_{RH} = 1$. The predictions of the strain development in comparison to the measured strains are on a satisfactory level for the first 120 days, so for the analysed period. The drying shrinkage in the wall was calculated using this formula for $t_s = 1 \text{ day}$, $h_0 = 600 \text{ mm}$.

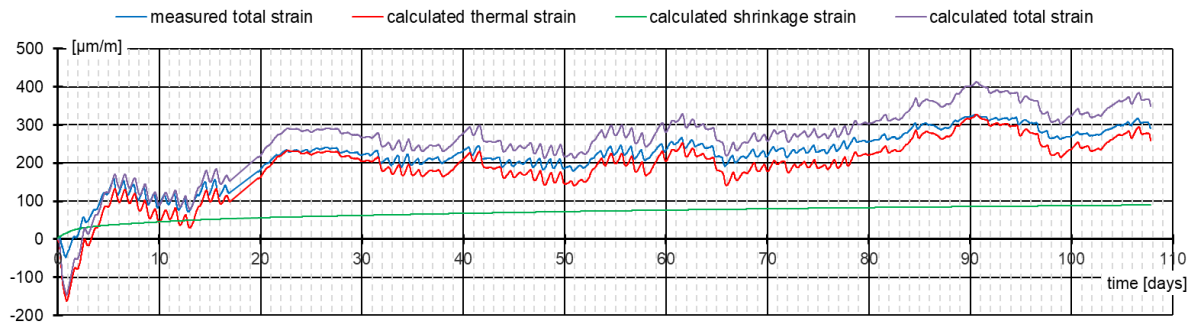


Figure A.14. Comparison between the measured and calculated strain at the level of + 5.40 m in the tank wall.

Figure A.14 shows comparison between the measured strain and the calculated strain in point B1, as well as the thermal strain and shrinkage strain in this location. It can be observed that the strain in the wall depends mostly on the thermal strain, which governs the behaviour of the strain change in time; thermal strain is also predicted to be about 4 times greater than the shrinkage strain. The calculated and measured strain in point B1 coincide quite well – significant difference is visible only at the stage of heating of the wall because the calculated strain does not take into account the effect of creep, which is known to be high in this period. The strains measured in point B1 can be treated as almost free strains and the free strain in the wall can be calculated with the above proposed approach.